ARTICLE IN PRESS
+ MODEL
Acta Pharmaceutica Sinica B xxxx;xxx(xxx):xxx

Chinese Pharmaceutical Association
Institute of Materia Medica, Chinese Academy of Medical Sciences

Acta Pharmaceutica Sinica B

www.elsevier.com/locate/apsb
www.sciencedirect.com

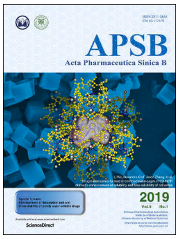

ORIGINAL ARTICLE

Dichotomous role of CD47−SIRPα axis: Leveraging opposing functions in phagocytic resistance and transport assistance for enhanced nanocarrier biocompatibility and tumor penetration

Xuehui Duan[a,b,†], **Yixuan Tang**[a,b,*,†], **Zhongjie Tang**[c], **Yan Du**[a,b], **Xinlei Chu**[a,b], **XinLong Liu**[c], **Zhanyan Liu**[d], **Kun Zhao**[d], **Wei Xu**[e,*], **Chong Li**[c,*]

[a] *School of Pharmaceutical Sciences & Institute of Materia Medica, National Key Laboratory of Advanced Drug Delivery System, Key Laboratory for Biotechnology Drugs of National Health Commission, Shandong First Medical University & Shandong Academy of Medical Sciences, Jinan 250117, China*
[b] *Medical Science and Technology Innovation Center, Shandong First Medical University & Shandong Academy of Medical Sciences, Jinan 250117, China*
[c] *Medical Research Institute, College of Pharmaceutical Sciences, Southwest University, Chongqing, 400715, China*
[d] *Department of Pharmaceutics, Key Laboratory of Chemical Biology (Ministry of Education), School of Pharmaceutical Sciences, Shandong University, Jinan 250012, China*
[e] *Shandong Provincial Qianfoshan Hospital, The First Hospital Affiliated with Shandong First Medical University, Jinan 250014, China*

Received 3 July 2025; received in revised form 19 September 2025; accepted 22 October 2025

KEY WORDS

Liposome;
Polyethylene glycol;
Accelerated blood clearance phenomenon;

Abstract Polyethylene glycol (PEG) carriers can improve drug circulation, but encounter biocompatibility and tumor penetration challenges. The CD47−SIRPα interaction on macrophages can initiate a “don’t-eat-me” signal, inhibiting phagocytosis. This study elucidates the dichotomous role of the CD47−SIRPα axis in conferring phagocytosis resistance and transport assistance for enhanced nanocarrier biocompatibility and tumor penetration. Using CD47-functional peptide, we elucidated the capacity of this axis to preserve carrier-cell membrane accessibility, impede macrophage-mediated nanocarrier

---

*Corresponding authors.

E-mail addresses: tangyixuan@sdfmu.edu.cn (Yixuan Tang), weixu@sdu.edu.cn (Wei Xu), chongli@swu.edu.cn (Chong Li).

[†] These authors made equal contributions to this work.

Peer review under the responsibility of Chinese Pharmaceutical Association and Institute of Materia Medica, Chinese Academy of Medical Sciences.

https://doi.org/10.1016/j.apsb.2025.11.013

2211-3835 © 2025 The Authors. Published by Elsevier B.V. on behalf of Chinese Pharmaceutical Association and Institute of Materia Medica, Chinese Academy of Medical Sciences. This is an open access article under the CC BY-NC-ND license (http://creativecommons.org/licenses/by-nc-nd/4.0/).

Please cite this article as: Duan Xuehui et al., Dichotomous role of CD47−SIRPα axis: Leveraging opposing functions in phagocytic resistance and transport assistance for enhanced nanocarrier biocompatibility and tumor penetration, Acta Pharmaceutica Sinica B, https://doi.org/10.1016/j.apsb.2025.11.013

CD47;
Endothelial cell;
Tumor microenvironment

endocytosis, reduce the secretion of IgG and IgM antibodies, and attenuate complement cascade activation. These mechanisms collectively neutralize the accelerated blood clearance of PEGylated liposomes. Notably, we identified the presence of SIRPα in endothelial vasculature and, for the first time, verified its pivotal role in orchestrating liposomal transit across the endothelial barrier. Moreover, within the tumor region, the CD47−SIRPα axis facilitated carrier hitchhiking on macrophages, enabling deep penetration into the tumor parenchyma and regulating the tumor microenvironment through the differential recognition of M1/M2-type tumor-associated macrophages. This study presents the first evidence of the dichotomous role of the CD47−SIRPα axis in regulating carrier biocompatibility, offering insights into its function to overcome the tumor permeability barrier challenge.

© 2025 The Authors. Published by Elsevier B.V. on behalf of Chinese Pharmaceutical Association and Institute of Materia Medica, Chinese Academy of Medical Sciences. This is an open access article under the CC BY-NC-ND license (http://creativecommons.org/licenses/by-nc-nd/4.0/).

1. Introduction

Over the past few decades, the integration of nanotechnology in cancer therapeutics has witnessed substantial growth[1-4]. Nonetheless, the quest for optimal therapeutics is hindered by persistent challenges, such as inadequate accumulation of these nanotherapeutics at their intended sites[5-7]. This challenge highlights the necessity to overcome the inherent barriers posed by the mononuclear phagocyte system, which significantly efficacy the circulation time of nano-carriers and consequently diminishes the clinical efficacy of these interventions[8,9]. One prominent strategy for prolonging the circulation of nanoparticles involves coating them with polyethylene glycol (PEG), a technique that has demonstrated success in extending their *in vivo* residence[10]. However, it triggers immunogenicity, leading to accelerated blood clearance (ABC) through the induction of antibody (*e.g.*, IgG and IgM) secretion and complement activation[11,12]. Consequently, refinement of carrier biocompatibility emerges as a pivotal pursuit in the quest for efficacious drug conveyance[13,14].

In addition, the limited infiltration of nanomedicines into solid tumors present another significant barrier to their therapeutic efficacy[15-17]. The enhanced permeability and retention (EPR) effect, which relies on the leaky vasculature characteristic of tumors to enhance drug accumulation, is often insufficient owing to the high interstitial pressure and heterogeneous vascular structures within tumors. Contemporary research elucidates the decisive role of endothelial cells in actively mediating nanoparticle transit[6,18,19]. To overcome this, ligand-based targeting of the tumor vasculature, such as the strategic incorporation of RGD peptides to engage $\alpha_v\beta_3$ integrin receptors on carrier exteriors, has proven advantageous for improving delivery specificity[20]. However, despite the promise of targeted delivery, such ligand-receptor interactions can inadvertently guide nanoparticles toward lysosomes within cells, where they are subject to degradation before reaching their intended intracellular targets[21]. Moreover, even upon successful extravasation from the tumor vasculature, nanocarriers must navigate a labyrinth of cellular barriers and dense extracellular matrix to penetrate deep into the tumor parenchyma[22,23]. Therefore, addressing these challenges is crucial for advancing the use of nanomedicines in cancer therapy.

The interaction between CD47 and signal regulatory protein α (SIRPα) plays a crucial role in immune regulation[24,25]. CD47, a ubiquitously expressed glycoprotein found on the surface of diverse cell types, including erythrocytes, platelets, and tumor cells, serves as a “don’t-eat-me” signal when it interacts with SIRPα[26]. SIRPα is predominantly expressed on myeloid cells, such as macrophages and dendritic cells, and to a lesser extent, on specific lymphocyte populations. The direct binding of these two proteins occurs *via* the extracellular domains. Notably, the cytoplasmic tail of SIRPα harbors two immunoreceptor tyrosine-based inhibition motifs (ITIM). Upon engagement with CD47, this ITIM domain undergoes phosphorylation, leading to the transmission of an inhibitory signal that effectively attenuates the phagocytic activity of macrophages, thereby safeguarding target cells from immune-mediated destruction. Moreover, studies have highlighted that the interaction between CD47 and the highly expressed SIRPα receptor on thymic endothelial cells can modulate VE-cadherin endocytosis through the ITIM−SHP2−Src signaling pathway, facilitating the opening of cellular junctions[27]. Additionally, the CD47−SIRPα axis has been recognized as a critical mediator of the transmigration of monocytes across the brain endothelial barrier[28,29]. Base on the foundational understanding of the role of CD47, researchers have engineered active peptides, termed self-peptide[25], that replicate the functionality of CD47. Self-peptides have demonstrated the ability to mimic CD47 binding to SIRPα and transmit an equivalent inhibitory signal, elucidating the therapeutic potential of self-peptide in modulating immune responses.

Based on the functions of CD47/self-peptide, they are widely regarded as capable of promoting the prolonged circulation of carriers[25,26,30]. Unlike PEG, which primarily exerts its effect through direct steric hindrance and cellular repulsion, our research indicates that the CD47−SIRPα axis possesses the unique ability to maintain the accessibility of carrier surfaces to their biological environment. Furthermore, the CD47−SIRPα axis has been proven to play a critical role in facilitating the transendothelial migration of monocytes; however, its application in enhancing the permeability of carriers remains unexplored. Considering these findings, we propose a synergistic fusion strategy that combines PEGylation with CD47-derived self-peptide to prolong the circulation time of the nanocarriers and improve their delivery efficiency. Using the CD47−SIRPα interaction, we hypothesize that it is possible to reduce macrophage-mediated phagocytosis and mitigate the antigen-presenting activity of phagocytes, thereby suppressing the *in vivo* immune responses. Although the EPR effect in tumors is considered a significant factor contributing to the accumulation of nanomedicines, active transport by endothelial cells is believed to dominate the process[19]. Therefore, we investigated the role of the CD47−SIRPα axis in mediating the transendothelial delivery of liposomes. Additionally, macrophages are recognized as key mediators of nanoparticle penetration into tumors[31]. Given that the CD47−SIRPα axis maintains

Please cite this article as: Duan Xuehui et al., Dichotomous role of CD47−SIRPα axis: Leveraging opposing functions in phagocytic resistance and transport assistance for enhanced nanocarrier biocompatibility and tumor penetration, Acta Pharmaceutica Sinica B, https://doi.org/10.1016/j.apsb.2025.11.013

accessibility to macrophages while inhibiting further phagocytosis, we hypothesized that this may also positively influence the penetration of drugs into the tumor regions (Scheme 1).

2. Materials and methods

2.1. Materials

Egg Lecithin Phosphatidylcholine (EPC, Cat# N01006), Cholesterol (CHO, Cat# O01001), DSPE-mPEG$_{2000}$ (Cat# F01008) and DSPE-PEG$_{2000}$-NHS (Cat# F02008) were provided by A.V.T. Pharmaceutical Tech Co., Ltd. (Shanghai, China). Egg Liss Rhod PE EPC (Cat# IO-000811) were purchased from Avanti Polar Lipids, Inc. (Alabaster, USA). Hoechst 33342 (Cat# H4079), DiOC18(3) (DiO, Cat# D4027), DiIC18(3) (DiI, Cat# D4010), DiIC18(5) (DiD, Cat# D4019), DiIC18(7) (DiR, Cat# D4006), and 5(6)-CFDA (Cat# C4037) were supplied by US Everbright Inc. (Suzhou, China). Mouse IgM (Cat# BDEL-0312) was provided by Biodragon Immunotechnologies Co., Ltd. (Beijing, China). 8-Hydroxypyrene-1,3,6-trisulfonic acid trisodium salt (HPTS, Cat# 01100310), Protease and Phosphatase Inhibitor Cocktail (100x) (Cat# 041729396) and RIPA Lysis Buffer (Medium) (Cat# 041127048) were purchased from Adamas life (Shanghai, China). Chlorpromazine (Cat# 71033) was from TM standard Company (Beijing, China). Colchicine (Cat# ST07260120) was provided by Nature standard Biotechnology Co., Ltd. (Shanghai, China). Filipin (Cat# HY-N6718) was from MCE Co., Ltd. (Shanghai, China). Protein A + G Agarose (Cat# P2055), LPS (Cat# S1732), IL-4 (Cat# P5129), and IFN-γ (Cat# P5664) were from Beyotime Biotechnology (Jiangsu, China). The antibodies used in this study are listed in (Supporting Information Table S1) of supporting information, and all other chemicals and reagents were of analytical grade.

2.2. Cell lines and animals

RAW264.7, bEnd.3, and 4T1 cells were purchased from Procell Life Science&Technology Co., Ltd. (Wuhan, China). All cells were cultured in Dulbecco's modified Eagle's medium (DMEM) (Adamas-life, China) supplemented with 10% fetal bovine serum (FBS) (Adamas-life, China), and detached for passage using 0.25% Trypsin/0.5 mM EDTA.

Female BALB/c mice (6−8 weeks old, 18−22 g) were provided by Jinan Pengyue Experimental Animal Breeding Co., Ltd. (Jinan, China). All animals were raised in an SPF laboratory environment with a 12 h light−dark cycle at 22−24 °C and 30%−50% relative humidity. All animal experiments were performed under the relevant guidelines and regulations of the Ethical Review Committee of Shandong Academy of Medical Sciences (Number: 20210135).

2.3. Synthesis of peptides

The self-peptide (sequence: GNYTCEVTELSREGKTVIELK), palmitate-modified self-peptide (sequence: Pal-GNYTCEVTELSREGKTVIELK), and RGD peptide (sequence:

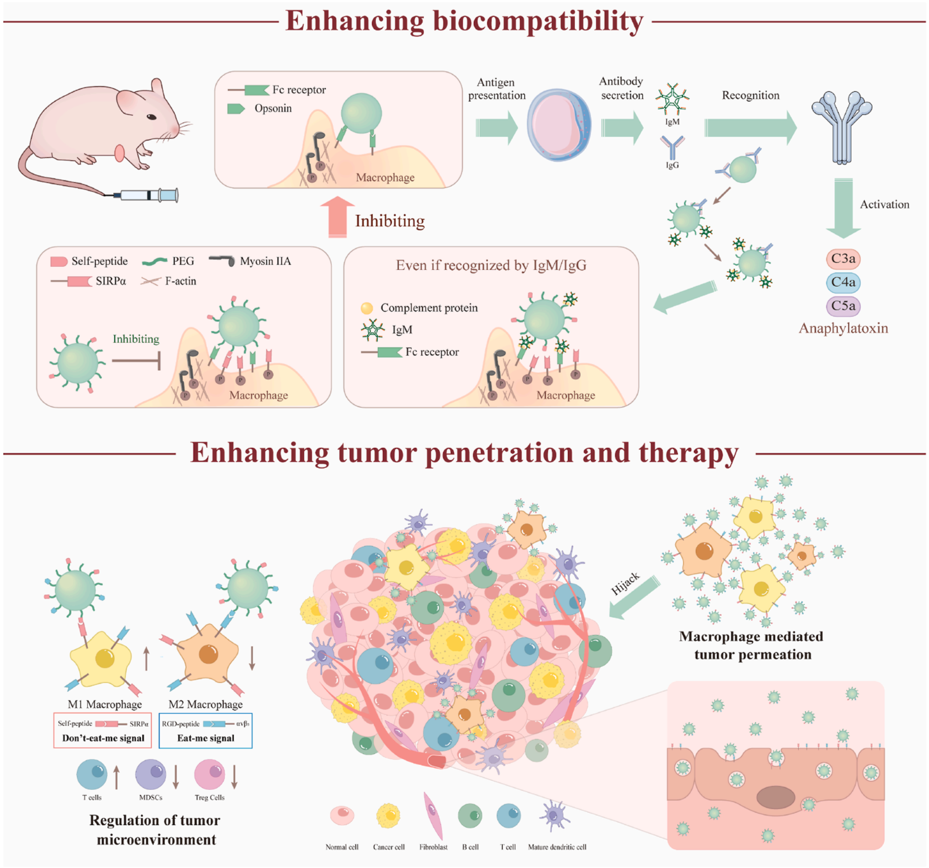

Scheme 1 Sequence recognition of the CD47−SIRPα axis in macrophages and endothelial cells can overcome the immunogenicity of PEGylated carriers and the barrier to tumor penetration.

Please cite this article as: Duan Xuehui et al., Dichotomous role of CD47−SIRPα axis: Leveraging opposing functions in phagocytic resistance and transport assistance for enhanced nanocarrier biocompatibility and tumor penetration, Acta Pharmaceutica Sinica B, https://doi.org/10.1016/j.apsb.2025.11.013

c(RGDYK)) were synthesized using solid-phase peptide synthesis with Fmoc-protected amino acids. After synthesis, the peptides were purified by reverse-phase high-performance liquid chromatography.

2.4. Synthesis of DSPE-PEG$_{2000}$ modified peptides

To prepare the DSPE-PEG$_{2000}$-peptide conjugates, the peptides were combined at a molar ratio of 1.3:1 with DSPE-PEG$_{2000}$-NHS. The mixture was then dissolved in a solution consisting of equal amounts of DMF and water, and *N*-methylmorpholine was added to adjust the pH to 8.0. The solution was stirred for 24 h at 600 rpm and maintained at 25 °C to facilitate conjugation. Following the reaction, the resulting solution was subjected to dialysis using a dialysis membrane with a molecular weight cutoff of 3500 Da and distilled water as the dialysis medium. After 24 h of dialysis, the solution was lyophilized for an additional 24 h. The obtained conjugates were verified using MALDI-TOF-MS (Autoflex speed, Bruker, Germany) and stored at −20 °C for later use.

2.5. Preparation of liposomes

Liposome fabrication was carried out employing the method of thin-film hydration[32]. The initial step entailed preparing a lipid mixture consisting of egg phosphatidylcholine (EPC) and cholesterol (CHO) in a 1:1 molar ratio, with detailed lipid composition ratios provided in (Supporting Information Table S2) for comprehensive insight. To this blend, fluorophores were introduced for labeling purposes: Egg Liss Rhod PE EPC, DiI, DiD, or DiR, each incorporated at precise quantities relative to EPC—40 μg of Egg Liss Rhod PE per 8 mg of EPC, 5 μg of DiI or DiD per 8 mg of EPC, and 20 μg of DiR per 8 mg of EPC, respectively. Following the meticulous addition of these fluorescent markers, the lipid mixture was subjected to vacuum evaporation to form a thin film. Subsequently, the dried lipid film underwent rehydration with phosphate-buffered saline (PBS) at 37 °C, reviving the lipids into a suspension. Subsequently, ultrasonication was performed in an ice water bath, followed by sequential extrusion through a polycarbonate membrane with a pore size of 100 nm to form liposomes.

For liposomes loaded with doxorubicin (DOX), the lipid film was hydrated with 250 mmol/L ammonium sulfate at 37 °C following the same procedure mentioned above. Subsequently, the liposomes were dialyzed (molecular weight cutoff of 8000−14,000 Da) using distilled water for 2 h. DOX was added to the liposomes at a ratio of 1:10 (*w*/*w*) and incubated at 56 °C for 1 h. The liposome/DOX formulation was dialyzed (molecular weight cutoff of 8000−14,000 Da) with PBS and stored at 4 °C until use. To analyze the encapsulation efficiency and drug loading, liposomes were isolated and placed in the upper chamber of a 1 mL ultrafiltration centrifuge tube. The tubes were centrifuged at 6000 rpm for 30 min, and the mass concentration of DOX was measured in both the liposome suspension and the filtrate collected from the lower chamber of the tube. A standard curve for DOX was constructed using a fluorescence spectrophotometer at an excitation wavelength of 470 nm and an emission wavelength of 580 nm. The Encapsulation Efficiency (%) was calculated using Eq. (1):

$$\text{Encapsulation efficiency (\%)} = \text{DOX(supernatant)}/\text{DOX(total)}$$

where DOX(total) (mg/mL) represents the initial amount of DOX added and DOX(supernatant) represents the concentration of DOX in the supernatant[33].

The Nano ZS 90 instrument from the Zeta Sizer Nano Series (Nano ZS, Malvern, UK) was employed to evaluate the size distributions of the synthesized liposomes through dynamic light scattering measurements.

2.6. Immunogenicity of liposomes

To evaluate the immunogenicity of P-Lip, SP-Lip, RP-Lip, and SRP-Lip, four doses of liposomes at 50 mg/kg per week were injected into BALB/c mice *via* the tail vein. Blood was collected after the 4th injection, and plasma was centrifuged at 1000 × *g* for 10 min (H1750R, Xiangyi, Changsha). Antibodies were detected by enzyme-linked immunosorbent assay using DSPE-mPEG$_{2000}$, DSPE-PEG$_{2000}$-self, or DSPE-PEG$_{2000}$-RGD as antigens (dissolved in ethanol). Microtiter plates were coated with antigen (2 μg per well) overnight. The plates were then rinsed with PBS and closed with 1% BSA for 1 h. Blood samples were serially gradient diluted with PBS and incubated in microtiter wells for 1 h. After rinsing with PBS, horseradish peroxidase-labeled goat anti-mouse IgG antibody was added to react with IgG. Blood samples were incubated for 1 h in microtiter wells. 3,3′,5,5′-Tetramethylbenzidine (TMB) was added for 5−15 min and the reaction was terminated with 2 mol/L sulfuric acid. UV absorption was detected at 450 nm (Varioskan LUX, Thermo Scientific, USA). For the determination of anti-PEG IgM, a similar ELISA protocol was employed, with the notable difference being the exclusive use of DSPE-mPEG$_{2000}$ as the antigen across all steps[34].

2.7. Complement activation assay

Liposomes (100 μL) containing 10 mmol/L lipid were incubated with 100 μL of pretreated mouse serum at 37 °C for 1 h. IgM was inactivated with 0.2 mol/L β-mercaptoethanol (37 °C, 1 h), and then recovered by addition of normal mouse IgM (37 °C, 1 h), and complement activation was quantitatively determined using a mouse C5a ELISA kit[34].

2.8. Analysis of co-localization of liposomes with liver and splenocytes in vivo

Liposomes labeled with DiI were delivered to mice through the tail vein. After a 4 h period, the mice were anesthetized, and cardiac perfusion with cold PBS was performed to eliminate blood, followed by removal of the liver and spleen. For flow cytometry analysis, specific cell-surface markers were targeted using fluorophore-conjugated antibodies. To detect macrophages, anti-F4/80 and anti-CD11b antibody was employed, while anti-CD19 antibody was used to identify B lymphocytes. The cell suspensions were subjected to a 30-min incubation at 4 °C with these antibodies to facilitate specific binding. After staining, the cells were washed twice with PBS to eliminate any unbound antibodies. Flow cytometry (Cytek Aurora, Cytek Biosciences,

Please cite this article as: Duan Xuehui et al., Dichotomous role of CD47−SIRPα axis: Leveraging opposing functions in phagocytic resistance and transport assistance for enhanced nanocarrier biocompatibility and tumor penetration, Acta Pharmaceutica Sinica B, https://doi.org/10.1016/j.apsb.2025.11.013

USA) analysis was performed to identify and quantify the various cell populations present in the samples[6].

2.9. Protein corona analysis

Four types of liposome injections, P-Lip, SP-Lip, RP-Lip, and SRP-Lip, were administered to BALB/c mice at a dosage of 50 mg/kg per week through the tail vein. After the fourth injection, blood samples were collected. Plasma was then obtained by centrifuging the blood at 1000 × *g* for 10 min. Next, 100 μL of liposomes containing 10 mmol/L lipids was combined with 100 μL of pretreated mouse serum and incubated at 37 °C for 1 h. Subsequently, the mixture was centrifuged at 12,000 × *g* for 1 h. The resulting precipitate was then washed with PBS and boiled for 10 min in the presence of a phosphoproteinase inhibitor. Finally, the sample was analyzed using LC−MS/MS (tims TOF Pro/UltiMate 3000 RSLC nano, Themo, USA)[34].

2.10. Endothelial cells transport efficiency

The bEnd.3 cell line was plated into Transwell inserts at a density of 10,000 cells/mL and cultured until their transendothelial electrical resistance (TEER) reached a minimum value of 150 Ω cm^2 (RE1600, Jin gong hong tai Technology, Beijing)[35]. Subsequently, DiD (0.5 μg/mL)-loaded liposomes were introduced into the upper chamber of the Transwell inserts. Samples (200 μL) of the medium from the lower chamber were collected at predetermined time intervals, and fluorescence intensity was measured using a fluorescence microplate reader (Varioskan LUX, Thermo Scientific, USA) set at an excitation wavelength of 595 nm and an emission wavelength of 665 nm.

2.11. MTT assay

For the MTT assay, 4T1 cells were seeded in 96-well plates (5×10^3 cells/well). After overnight culture, the cells were treated with free DOX, DOX-loaded liposomes, or empty liposomes for 24 h. The culture media was then removed and replaced with fresh complete medium containing MTT solution (final concentration was 0.5 mg/mL). Following incubation for 4 h, the medium was removed and the formazan crystals were dissolved in 150 μL of DMSO. The absorbance of each well was measured at 490 nm using a microplate reader (Varioskan LUX, Thermo Scientific, USA).

For macrophages, cells were first polarized by pre-incubation with either interferon-gamma (IFN-γ, 20 ng/mL) and lipopolysaccharide (LPS, 100 ng/mL) for M1 polarization or interleukin-4 (IL-4, 20 ng/mL) for M2 polarization for 24 h. After polarization, the macrophages were seeded in 96-well plates at a density of 5×10^3 cells per well and cultured overnight under the same conditions as the 4T1 cells. Following this, the macrophages were treated and processed for the MTT assay in the same manner as the 4T1 cells[36].

2.12. Penetration assay of the liposomes in 3D tumor spheroids

4T1 cells (5×10^5 cells/mL) were added to a 2% agarose-coated Petri dish and grown at 37 °C. The growth of spheroids was monitored using an EVOS fluorescence microscope (M5000, Thermo Scientific, USA). Once the spheroid size reached ∼800 μm, 5(6)-CFDA labeled RAW264.7 were added and co-culture with spheroid for another 4 h. Then Liss rhod PE EPC-labeled liposomes were added, and the spheroids were cultured for an additional 2 h. Afterward, the spheroids were washed, and the fluorescence was measured using a confocal microscope (Cell discoverer 7, Zeiss, Germany) with an XY-stack and 30 μm intervals.

2.13. In vivo anticancer assessment

BALB/c mice were inoculated subcutaneously with a sufficient amount (5×10^6) of 4T1 cells. When the tumor volume reached ∼200 mm^3, the mice were randomly divided into six groups ($n = 6$/group): i) PBS, ii) DOX, iii) P-Lip/DOX, iv) SP-Lip/DOX, v) RP-Lip/DOX, and vi) SRP-Lip/DOX. The dose of DOX was 5 mg/kg, and drug administration was performed on Days 0, 3, 7, and 10 through the tail vein. The tumor volume [length × $(\text{width})^2$ × 1/2] and body weight of different groups were measured every two days.

2.14. In vivo and ex vivo fluorescence image

BALB/c mice were inoculated subcutaneously with a sufficient amount (5×10^6) of 4T1. When the tumor volume reached ∼500 mm^3, DiR loaded liposomes were injected into the mice *via* the tail vein. Fluorescence images were collected at predetermined time points using the VISQUE *in vivo* Smart-LF System (Vieworks, Korea). At the end point (24 h), the mice were sacrificed for ex vivo imaging.

2.15. 3D fluorescence imaging of liposomes in tumors

After injecting DiI-loaded liposomes, the tumors were carefully removed from the mice and fixed in 4% PFA for 24 h. To decolorize the samples, quadrol decolorization solution was used for 2 days, followed by treatment with 5% ammonium solution at 37 °C in a shaker. For delipidation, the samples were placed in gradient tB delipidation solutions for 2 days and then in tB-PEG for 2 days for dehydration. The samples were then immersed in BB-PEG medium at 37 °C for at least one day for clearing. The livers were observed using a Light Sheet Fluorescence Microscope (LSFM, Nuohai LS 18, Beijing). The acquired images were then reconstructed and analyzed using Imaris software (Bitplane) [37].

2.16. Analysis of co-localization of liposomes and cells in tumors

Liposomes labeled with DiI were administered to mice *via* the tail vein. Four hours later, the mice were anesthetized and subjected to cardiac perfusion with cold PBS to eliminate blood, followed by tumor removal.

For flow cytometry analysis, specific cell-surface markers were targeted using fluorophore-conjugated antibodies. To identify macrophages, anti-CD45 and anti-F4/80 antibodies were used, while anti-CD45 and anti-CD3 antibodies were used to identify T lymphocytes. Anti-CD45 and anti-CD11b and anti-Gr1 antibodies were used to identify myeloid-derived suppressor cells (MDSCs). The cell suspensions were subjected to a 30-min incubation at 4 °C with these antibodies to facilitate specific binding. After staining, the cells were washed twice with PBS to eliminate any unbound antibodies. Flow cytometry analysis (Cytek Aurora, Cytek Biosciences, USA) was performed to identify and quantify the various cell populations present in the samples.

For fluorescence imaging, the excised tumors were sectioned at 10 μm and subsequently labeled with macrophages using the F4/80 antibody and endothelial cells using the CD31 antibody,

Please cite this article as: Duan Xuehui et al., Dichotomous role of CD47−SIRPα axis: Leveraging opposing functions in phagocytic resistance and transport assistance for enhanced nanocarrier biocompatibility and tumor penetration, Acta Pharmaceutica Sinica B, https://doi.org/10.1016/j.apsb.2025.11.013

followed by the addition of fluorescence-labeled secondary antibodies. The resulting samples were analyzed using a confocal microscope (Celldiscoverer 7, Zeiss, Germany).

2.17. Immunohistochemical analysis

Anticancer therapy was performed as described in the *in vivo* anticancer assessment. On Day 14, mice were sacrificed, and tumors were carefully removed. For immunohistochemical analysis, collected tumors were fixed with 4% PFA, sectioned, and stained with hematoxylin and eosin (H&E) or Tunel.

2.18. Quantification of tumor-infiltrating lymphocytes

Tumor tissues were obtained following the protocol described in the *in vivo* anticancer assessment section. To prepare cell suspensions, the obtained tumor tissues were first ground and then passed through a 200-mesh sieve. The cell suspensions were then co-incubated with antibodies for T cell staining (CD45, CD3, CD4, and CD8), myeloid-derived suppressor cell staining (Gr1, CD11b, and CD45), macrophage staining (CD45, F4/80, CD86 or CD206), and Treg (CD45, CD3, CD4, and FOXP3) for FACS analysis (Cytek Aurora, Cytek Biosciences).

2.19. Statistical analyses

Results are expressed as means ± standard deviation (SD). Data were analyzed by one-way analysis of variance (ANOVA) followed by Tukey's test and $P < 0.05$ was considered statistically significant.

3. Results and discussion

3.1. Self-peptide-attached liposomes (S-Lip) induce the "don't-eat-me" signal while preserving accessibility to macrophages

Our initial investigation centered on differentiating the distinctive impact of the CD47-SIRPα axis from that of conventional PEGylated liposomes in regulating the dynamics of liposome-macrophage interactions. The self-peptide is a bioactive fragment extracted from the CD47 protein, with an established proficiency to replicate the complete functionality of CD47 and effectively engage SIRPα[25,32]. Furthermore, we confirmed that the *in vivo* administration of peptide did not elicit significant immunogenicity (Supporting Information Fig. S1). Therefore, we engineered a palmitoylated derivative of the self-peptide (sequence: palmitic acid-GNYTCEVTELSREGKTVIELK) (Supporting Information Fig. S2), where the palmitic acid moiety served as an anchor, promoting the stable integration of the peptide onto the liposome surface. Using the thin-film hydration methodology, we successfully conjugated this modified peptide to liposomes, yielding S-Lip. Through preliminary experiments, we optimized the self-peptide loading of S-Lip to a concentration of 1%[38]. To establish a comprehensive comparative framework, unmodified liposomes (Lip) and those modified with DSPE-mPEG$_{2000}$ at a molar ratio of 5% (P-Lip) were also prepared as control groups (Fig. 1A, Supporting Information Table S3).

Cytophagy is an energy-dependent process[39]. At 4 °C, the cells were unable to internalize the particles, and the interaction between liposomes and cells resulted only in surface adhesion [40]. As depicted in (Fig. 1B), following a 1 h co-culture at 4 °C, quantitative analysis revealed significantly reduced adherence of P-Lip to macrophage surfaces compared to both unmodified Lip and S-Lip formulations, with no substantial difference observed between the latter two groups. This observation elucidates the effectiveness the classic PEGylation strategy in reducing serum protein adsorption and subsequent macrophage attachment through the creation of a slippery surface, whereas S-Lip, despite its surface modifications, retained an affinity for macrophage membranes akin to non-PEGylated liposomes. To visually confirm these interactions, confocal microscopy was used (Fig. 1C). Over a 2 h timeframe, Lip was rapidly internalized by macrophages, reflecting efficient endocytosis. While demonstrating reduced uptake, P-Lip still exhibited noticeable cytoplasmic accumulation (indicated by white arrows). Conversely, S-Lip displayed susceptibility to robust membrane associations (highlighted by orange arrows), supporting its role in enhancing surface adherence, without triggering extensive endocytosis.

To clarify the distinction between surface adhesion and phagocytosis, macrophages were cultured at 4 °C to inhibit endocytosis and at 37 °C to permit it; then cells were exposed to liposomes for 1 h. As illustrated in (Fig. 1D), the fluorescence intensity profiles of Lip and S-Lip were comparable at 4 °C, reinforcing the notion that self-peptide modification does not deter liposome attachment to the macrophages. Notably, at physiological temperature (37 °C), S-Lip appeared to mitigate macrophage phagocytosis, thereby influencing total cellular uptake levels.

3.2. "Don't-eat-me" signaling synergizes with PEG modification in the construction of biocompatible and efficient drug delivery systems

Based on the different roles of the CD47-SIRPα axis and PEG modification in regulating the interaction between liposomes and macrophages, we proposed that the co-modification of both could facilitate efficient liposome delivery. First, we synthesized DSPE-PEG$_{2000}$-self (Supporting Information Figs. S3-S5). RGD is a widely used tumor-targeting peptide, and we similarly synthesized DSPE-PEG$_{2000}$-RGD (Supporting Information Figs. S6 and S7). We then co-modified it with self-peptide on the liposome surface to assess the effect of targeting peptide binding on the *in vivo* behavior of liposomes.

Initially, we examined the influence of the molar ratio of self-peptides on the interaction between the liposomes and macrophages. With a 4 h incubation period, SP-Lip, in which 0.1−2% of DSPE-PEG$_{2000}$-self was incorporated, exhibited substantial anti-macrophage phagocytic effects. However, after 12 h of incubation, only self-peptide modified with more than 1% molar ratio maintained their anti-phagocytosis efficacy (Supporting Information Fig. S8). Furthermore, we conducted a preliminary investigation into the effects of the RGD peptide modification ratio. A higher RGD peptide modification ratio hindered endocytosis of the self-peptide, whereas the anti-phagocytosis effect of the self-peptide remained unaffected at a 1% modification ratio (Supporting Information Fig. S9). This could be because the receptor $\alpha_v\beta_3$ of the RGD peptide was also significantly expressed in macrophages (Supporting Information Fig. S10), and the recognition of the RGD peptide by $\alpha_v\beta_3$ will modulate the interactions with self-SIRPα, in turn affecting "don't-eat-me" signal activation. Moreover, L-type natural peptides are unstable *in vivo* and are prone to degradation by proteases[39]. We conducted related experiments by mixing liposomes modified with different ratios of peptides with serum at a 1:1 ratio and incubating the mixture at

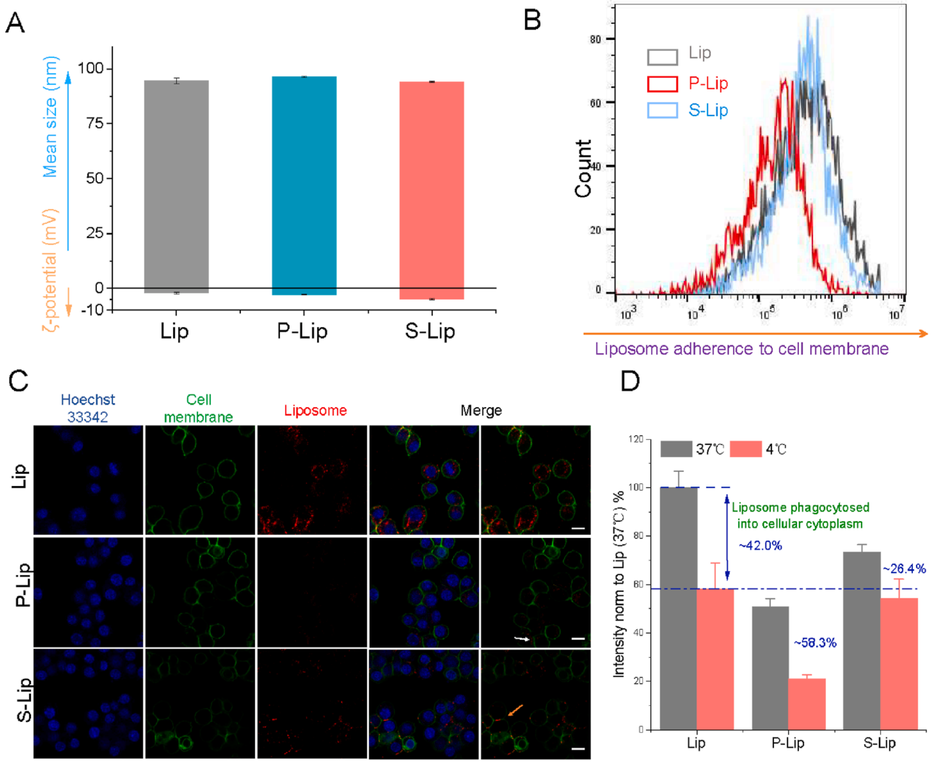

Figure 1 Characterization of the ability of self-peptide-attached liposomes (S-Lip) to delay macrophage phagocytosis. (A) Size distribution and zeta potential of liposomes. (B) Flow cytometric analysis of RAW264.7 cells incubated at 4 °C for 30 min, followed by liposomes for 1 h. (C) Confocal images of RAW264.7 cells incubated with liposomes for 2 h. Scale bar = 10 μm. The orange arrows indicate the adhesion of S-Lips to the cell membrane. (D) Flow cytometric analysis of RAW264.7 cells incubated at 37 °C or 4 °C for 30 min, followed by liposomes for 1 h. Data are presented as the mean ± SD ($n = 3$). Lip, liposomes without surface modification; P-Lip, liposomes modified with DSPE-mPEG$_{2000}$; S-Lip, self-peptide-attached liposomes.

37 °C for 72 h. Our results showed that when the modification ratio of self-peptides lower than 1%, the anti-phagocytic effect of liposomes was significantly reduced (Supporting Information Fig. S11).

We then prepared several liposome formulations (Tables S2 and S3), namely P-Lip (liposomes modified with DSPE-mPEG$_{2000}$), SP-Lip (liposomes modified with DSPE-PEG$_{2000}$-self), RP-Lip (liposomes modified with DSPE-PEG$_{2000}$-RGD), and SRP-Lip (liposomes synergistic modified with DSPE-PEG$_{2000}$-RGD and DSPE-PEG$_{2000}$-self) (Tables S2 and S3, Supporting Information Fig. S12). The binding of CD47 to SIRPα initiates signal transmission to the four tyrosine residues located in the cytoplasmic domain of SIRPα, forming two ITIMs[28]. Upon signal transmission, these tyrosine residues undergo phosphorylation and subsequently recruit and activate the cytoplasmic tyrosine phosphatases SHP-1 and SHP-2. SHP-1 and SHP-2 dephosphorylate or downregulate a series of substrates, thereby inhibiting the phagocytic capacity of macrophages[25,26,41]. Consequently, the degree of SIRPα phosphorylation serves as a critical indicator of whether the self-peptide can inhibit macrophage phagocytosis and provides a foundation for further experimentation[42]. As illustrated in (Supporting Information Fig. S13), we analyzed the expression levels of SIRPα and phosphotyrosine SIRPα utilizing immunoprecipitation in conjunction with western blotting. The relative phosphorylation level of SIRPα tyrosine were compared between liposome-treated and control groups. No significant difference was observed in the expression of phosphotyrosine SIRPα in the P-Lip and RP-Lip groups compared with that in the control group. However, the relative phosphorylation levels of SIRPα tyrosines in the SP-Lip and SRP-Lip groups increased by 1.56-fold and 1.41-fold, respectively, compared to the control group. These findings confirmed that both designed peptides successfully initiate the SIRPα tyrosine phosphorylation pathway in macrophages. Subsequently, we co-incubated the liposomes with RAW264.7 macrophages. After 2 h incubation (Fig. 2A), the endocytosis of SP-Lip by macrophages was reduced, compared to that of P-Lips, which indicated a synergistic effect of "don't-eat-me" signaling and PEG modification. As for $\alpha_v\beta_3$ expression on the macrophage surface, RP-Lip and SRP-Lip adsorption to the macrophage surface was significantly increased after modification with RGD peptides. However, the number of macrophages that endocytosed SRP-Lips was significantly lower than that endocytosed by RP-Lip. Furthermore, we conducted additional incubations at 4 °C and 37 °C to quantitatively analyze macrophage endocytosis. As depicted in (Fig. 2B−D), the adsorption of P-Lip and SP-Lip was comparable, but SP-Lip uptake was significantly lower than P-Lip uptake at 37 °C, confirming that SP-Lip inhibits cellular uptake by reducing macrophage endocytosis. The adsorption of both RP-Lip and SRP-Lip on the cell membrane surface was significantly higher than that of P-Lip at 4 °C, confirming that RGD peptide modification increased the interaction between liposomes and the cell membrane surface. At 37 °C, RP-Lip uptake was significantly

Please cite this article as: Duan Xuehui et al., Dichotomous role of CD47−SIRPα axis: Leveraging opposing functions in phagocytic resistance and transport assistance for enhanced nanocarrier biocompatibility and tumor penetration, Acta Pharmaceutica Sinica B, https://doi.org/10.1016/j.apsb.2025.11.013

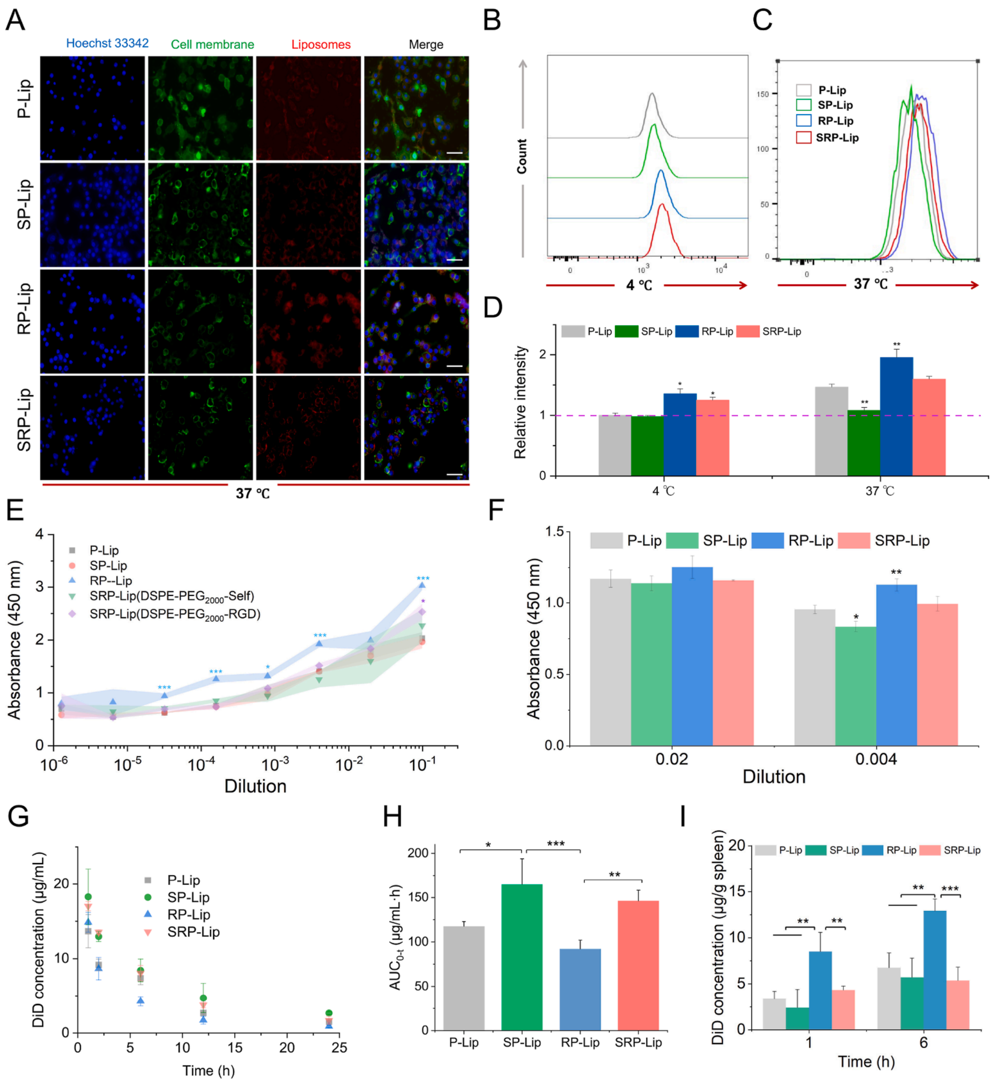

Figure 2 "Don't-eat-me" signal enhances liposomal biocompatibility. (A) Fluorescence imaging of liposomes with RAW264.7 cells after 2 h of co-incubation, scale bar = 5 μm. (B-D) Flow cytometric analysis of RAW264.7 cellular uptake of different liposomes. Cells were pre-incubated at (B) 4 °C and (C) 37 °C for 30 min, and then, liposomes were added and further incubated for 1 h, followed by (D) the quantification of liposome uptake using flow cytometry. (E) Changes in IgG and (F) IgM titers following the injection of different liposomes. (G) Plasma drug concentration after the injection of different liposomes, (H) Area under the curve (AUC) values, and (I) spleen distribution changes. Data are presented as the mean ± SD ($n = 3$), $^{*}P < 0.05$, $^{**}P < 0.01$, and $^{***}P < 0.001$. P-Lip, liposomes modified with DSPE-mPEG$_{2000}$; SP-Lip, liposomes modified with DSPE-PEG$_{2000}$-self; RP-Lip, liposomes modified with DSPE-PEG$_{2000}$-RGD; SRP-Lip, liposomes synergistic modified with DSPE-PEG$_{2000}$-RGD and DSPE-PEG$_{2000}$-self.

higher than P-Lip uptake, whereas SRP-Lip uptake did not differ significantly from P-Lip uptake. This result demonstrated that the enhanced liposome-cell surface interaction caused by RGD peptides did not inhibit the function of the self-peptide.

IgG and IgM levels in the blood were examined 12 h after liposome administration. As depicted in (Fig. 2E and F), RP-Lip resulted in higher IgG and IgM levels than the other liposome formulations. When DSPE-PEG$_{2000}$-RGD nanoparticles were used as the antigen, the antibody concentration in the SRP-Lip group was lower than that in the RP-Lip group, confirming that the "don't-eat-me" signaling pathway reduced the *in vivo* immunogenicity of DSPE-PEG$_{2000}$-RGD nanoparticles, thereby enhancing liposome biocompatibility. Additionally, we analyzed the pharmacokinetics of liposomes *in vivo* and found that the blood concentrations and area under the curve (AUC) values of SP-Lip were higher than those of P-Lip (Fig. 2G and H), further demonstrating the synergistic effect of co-modification from the perspective of *in vivo* bioavailability. Notably, the AUC values decreased after modification with the RGD peptide. This is because RGD peptide modification increase *in vivo* interaction with macrophages. As depicted in Fig. 2I, the splenic distribution of SRP-Lip was lower than that of RP-Lip, demonstrating that modifying the self-peptide inhibits B cell recognition and suppresses the immune response. Complement proteins can be activated by the complex formed by antibodies and antigens through the classical pathway, resulting in downstream products, such as C5a, which enhances recognition by macrophages and B cells and is also an important *in vivo* allergenic toxin[13,14,43]. We used an

Please cite this article as: Duan Xuehui et al., Dichotomous role of CD47—SIRPα axis: Leveraging opposing functions in phagocytic resistance and transport assistance for enhanced nanocarrier biocompatibility and tumor penetration, Acta Pharmaceutica Sinica B, https://doi.org/10.1016/j.apsb.2025.11.013

ELISA kit to measure complement protein concentrations, and found that the concentration of C5a was significantly lower in the SRP-Lip group than in the RP-Lip group (Supporting Information Fig. S14). These findings confirm that synergistic modification of the self-peptide reduces PEG liposome immunogenicity and the peptide synergizes with PEG to improve the *in vivo* circulation time of the carrier.

3.3. *"Don't-eat-me" signaling synergizes with PEG modifications to overcome the PEG-induced accelerated blood clearance phenomenon*

The clinical application of PEGylated liposomes is limited by ABC phenomenon. The enhancement of carrier recognition through the induction of IgM antibodies and the role of the complement system in carrier clearance mediated by immune cells are the main factors contributing to this phenomenon[44,45].

In our experiment, 1 μg/mL mouse IgM was added to fresh mouse serum, which was then combined with P-Lip, SP-Lip, RP-Lip, and SRP-Lip, each at a 1:1 ratio. This mixture was maintained at 37 °C for 1 h to allow potential antibody binding before being presented to RAW264.7 macrophage cells for incubation for an addition 2 h. A separate group of P-Lip that were not pre-incubated with serum served as a control (P-Lip (control)). The results are shown in (Supporting Information Fig. S15A-S15D) illustrated that P-Lip experienced significantly elevated uptake by RAW264.7, compared to the non-serum exposed P-Lip (control), suggesting that serum exposure, likely through IgM opsonization, augmented macrophage uptake. Conversely, SP-Lip, despite showing similar adherence to macrophages at 4 °C as P-Lip, demonstrated a marked reduction in uptake at 37 °C compared to both the P-Lip and P-Lip (control) groups.

Subsequently, we established an *in vivo* murine model to delve deeper into the immunological responses elicited by the different liposomal formulations. Notably, we observed a conspicuous elevation in both IgG and IgM antibody titers in mice administered P-Lip and RP-Lip, indicating a heightened immunogenic reaction. Conversely, SP-Lip and SRP-Lip, featuring self-peptide modification, manifested significantly reduced immunogenic profiles, as evidenced by the lower antibody levels (Fig. 3A and B). To further elucidate the implications of these findings, we assessed the pharmacokinetic behavior of the liposomal formulations *in vivo*. As illustrated in Fig. 3C and detailed in Supporting Information Table S4, AUC, a measure of drug exposure over time − for P-Lip was substantially decreased following the induction of the ABC effect, highlighting accelerated clearance from circulation. Conversely, the AUC values for SP-Lip and SRP-Lip remained relatively stable, indicating minimal variation if the ABC phenomenon was induced or not. These results collectively affirm the hypothesis that incorporating the self-peptide into the liposome surface not only reduces the immunogenicity typically associated with PEG and RGD peptide modifications but also fosters an environment conducive to prolonged liposome circulation in the bloodstream.

Delving further into the immunological consequences of post-ABC phenomenon induction, we analyzed the engagement between liposomes and key immune cells, specifically macrophages and B cells, in vital organs, such as the liver and spleen (Fig. 3D−F, Supporting Information Fig. S16). Our analyses revealed stark contrast in the affinities of various liposomal formulations for these cell populations. P-Lip and RP-Lip, which lack self-peptide modification, demonstrated significantly elevated uptake by hepatosplenic B cells, suggesting that they potentially elicit a stronger immune response. Conversely, SP-Lip and SRP-Lip, fortified with the self-peptide, showed reduced interaction with these cells, indicating a dampened immunogenic profile. The activation of the complement system *via* receptors on B cells is a pivotal step in the classical pathway of the immune response. By integrating self-recognition signals through SP-Lip and SRP-Lip, our data imply a strategic modulation of this cascade, suppressing antibody secretion and attenuating the immune response *in vivo*. This diminished immune activation not only restrains the production of antibodies that could trigger rapid clearance of the liposomes but also enhanced the compatibility of these nanocarriers with the host's immune system. These findings highlight the potential of self-peptide-modified liposomes as universal excipients that can be harnessed to augment the biocompatibility and safety profile of *in vivo* delivery systems.

3.4. *"Don't-eat-me" signaling synergizes with the PEG modification to reduce IgG and IgM levels and complement cascade activation*

To fully resolve the state of protein corona activity on the liposome surface, we extracted serum from various groups of mice after the induction of the ABC phenomenon, incubated them with liposomes, and isolated the corresponding protein coronas for proteomic analysis (Supporting Information Fig. S17). Functional analysis showed that liposomes were mainly covered by albumin and coagulation proteins (Fig. 4A). Moreover, complement and immunoglobulin components in the P-Lip and RP-Lip groups were significantly more abundant than those in the SP-Lip and SRP-Lip groups (Fig. 4B). shows the protein components with an abundance of >1% in the protein corona. In all four groups, the abundance of albumin was greater than 30%, which is attributed to albumin comprising approximately 60% of plasma proteins and its hydrophobic regions being attracted to the hydrophobic regions on the surfaces of the liposomes for stable binding.

In Fig. 4C−a detailed examination of the specific immunoglobulin components in the various liposome groups is presented. Notably, P-Lip and RP-Lip formulations exhibited a higher presence of proteins implicated in *in vivo* immunogenic recognition compared to their modified counterparts, SP-Lip and SRP-Lip. Among these, immunoglobulin heavy constant gamma 2 B (IGHG2B) is a key player. IGHG2B represents a distinct subclass of immunoglobulins, or antibodies that are, synthesized by B lymphocytes. It plays a pivotal role in the immune response by facilitating the generation of immune memory and constitutes a vital line of defense against a wide array of pathogens, including bacteria, viruses, and other foreign substances. The specificity of IGHG2B lies in its unique antigen-binding region, which allows it to selectively recognize and bind to antigens present on the surface of the liposomes. This binding process effectively 'tags' the liposomes, marking them for recognition by the immune system, particularly phagocytic cells such as macrophages. Consequently, liposomes coated with IGHG2B can elicit an immune response that leads to their clearance from circulation, thereby impacting their efficacy and longevity in the body. The differential immunoglobulin binding observed between the P-Lip/RP-Lip and SP-Lip/SRP-Lip formulations underscore the significance of surface modifications in modulating the immune response. Liposomes designed to minimize immunogenic interactions, such as SP-Lip and SRP-Lip, may exhibit improved biocompatibility and stealth

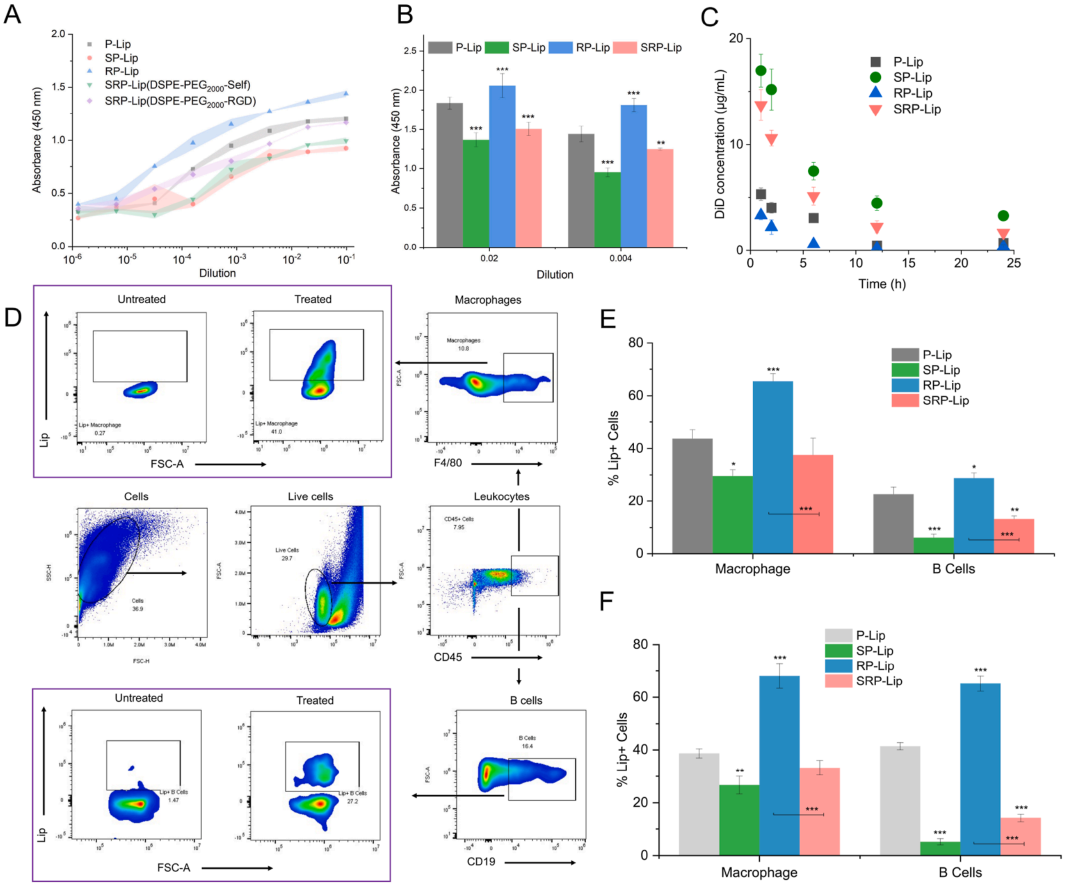

Figure 3 "Don't-eat-me" signaling inhibits the accelerated blood clearance phenomenon of PEGylated liposomes. Mice were first administered liposomes (50 mg/kg) once per week *via* the tail vein for 4 weeks to induce accelerated blood clearance. After the last administration, the model mice were analyzed for (A) IgG and (B) IgM antibody titers and (C) pharmacokinetic analysis. The colocalization of liposomes with macrophages and B cells in the (D and E) liver and (F) spleen was analyzed 4 h after the tail vein injection of DiI-labeled liposomes (50 mg/kg). Data are presented as the mean ± SD ($n = 3$), $^{*}P < 0.05$, $^{**}P < 0.01$, and $^{***}P < 0.001$.

properties, enhancing their potential for targeted drug delivery and minimizing unwanted immune activation.

Complement proteins are critical to the immune response and play a vital role in defense against infection, removal of cellular waste, and regulation of the immune response through various mechanisms[46]. The complement activation process involves stimulus recognition, cascade reactions, and the formation of membrane attack complex formation[47]. Generally, there are three pathways for complement activation, the classical, alternative, and lectin pathway. Compared with those in the SP-Lip and SRP-Lip groups, higher levels of complement and antibody components were found in the P-Lip and RP-Lip groups (Fig. 4D), which facilitates the classical complement cascade activation[48]. Additionally, the P-Lip and RP-Lip groups had higher concentrations of factors H and D, which enabled more efficient initiation of the alternative complement cascade[8]. Furthermore, the abundance of mannose-binding lectin in the P-Lip and RP-Lip groups exceeded 1%, which also provided a favorable environment for lectin complement pathway initiation[48,49]. In summary, the complement systems in the P-Lip and RP-Lip groups were efficiently activated through classical, alternative, and lectin pathways, leading to C3 convertase formation. This accelerates the recognition of complement receptors on macrophages and B cells[50]. In addition, we analyzed the plasma levels of complement protein C5a after inducing the ABC phenomenon in mice. The results, presented in (Supporting Information Fig. S18), demonstrate that the concentrations of C5a in the P-Lip and RP-Lip groups were significantly higher than those in the other groups, whereas a smaller change was noted in the SRP-Lip group. These data further validate the effectiveness of "don't-eat-me" signaling in enhancing liposome biocompatibility.

3.5. CD47−SIRPα axis facilitates liposome transport across the endothelial cell barrier

Overcoming the vascular endothelial cell barrier is vital for successful penetration of nanomedicines into tumor tissues[19]. Although the EPR effect has traditionally been hailed as the paramount mechanism behind nano-drug tumor accumulation, recent evidence has increasingly emphasized the pivotal role of endothelial cell transport in facilitating nano-drug penetration into tumors[19]. Strategies currently employed to overcome these barriers primarily involve receptor-mediated or adsorptive endocytosis[51]. Nonetheless, these methods have a significant drawback: high-affinity ligand-receptor binding frequently directs nanocarriers toward lysosomal degradation, thereby curtailing their therapeutic potential[21,52]. SIRPα, a critical ligand of CD47, is confirmed expressed in endothelial cells, and CD47-SIRPα

Please cite this article as: Duan Xuehui et al., Dichotomous role of CD47−SIRPα axis: Leveraging opposing functions in phagocytic resistance and transport assistance for enhanced nanocarrier biocompatibility and tumor penetration, Acta Pharmaceutica Sinica B, https://doi.org/10.1016/j.apsb.2025.11.013

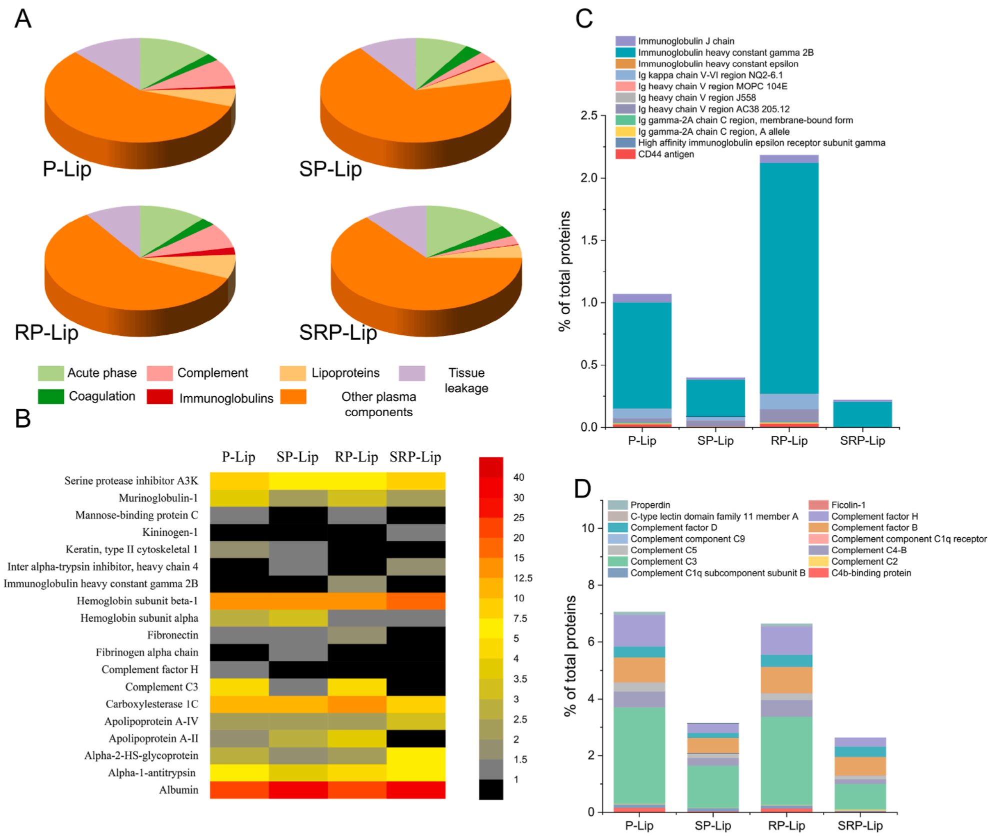

Figure 4 Proteomic analysis of liposomal protein corona. Mice were intravenously administered liposomes once per week (50 mg/kg) for four consecutive weeks to induce accelerated blood clearance. 12 h after the final administration, mouse plasma was co-incubated with liposomes at a 1:1 ratio at 37 °C for 1 h. Subsequently, the proteins adsorbed onto the liposomes were separated through centrifugation and analyzed *via* LC−MS/MS. (A) Classification of protein corona components. The identified proteins were categorized based on their involvement in biological processes, and the cumulative protein amounts were calculated. (B) Heat map illustrating the most prevalent proteins within the protein corona, as determined *via* proteomic mass spectrometry. Only proteins constituting at least 1% of the protein corona on any nanocarrier are shown. (C) Analysis of the proportion of immunoglobulin components among total proteins in the protein corona. (D) Analysis of the proportion of complement protein components among total proteins of the protein corona.

interactions can mediate transcytosis, a process that is independent of ligand-receptor dissociation (Fig. 5A)[27,29].

We initiated our investigation by confirming the expression of SIRPα and $\alpha_v\beta_3$ integrin in mouse brain microvascular endothelial cells bEnd.3 cell line (Fig. 5B and C, Supporting Information Fig. S19). Based on this validation, we carried out supplementary experiments to delve deeper into the endocytic behavior of various liposomal formulations within bEnd.3 cells (Fig. 5D−F). In contrast, SP-Lip and RP-Lip exhibited marginally elevated uptake rates compared with P-Lip. Notably, SRP-Lip demonstrated a substantially heightened cellular uptake, significantly surpassing the other three formulations. This observation points toward a synergistic impact arising from dual modification with both self- and RGD-peptides. In addition, colocalization studies with lysosomes revealed that RP-Lip displayed a considerably greater association with lysosomes (Fig. 5G and H). Conversely, lysosomal colocalization was notably reduced in the remaining three liposomal groups. Collectively, these results imply a protective role for the self-peptide in facilitating liposome evasion from lysosomal degradation during their intracellular transit, thereby enhancing their potential for effective translocation and bioavailability within target cells. To clarify the changes in the mechanism of liposome uptake by bEnd.3 cells after peptide modification, we analyzed the cellular uptake mechanism using the following four approaches: pre-incubating cells at 4 °C to inhibit the primary energy supply for transport[39]; using chlorpromazine to block the assembly of coated pits on the cell surface, thereby inhibiting clathrin-mediated endocytosis[53]; using colchicine to inhibit microtubule assembly, thus suppressing macropinocytosis[54]; and using filipin, which binds to cholesterol in caveolae, to inhibit caveolae-mediated endocytosis[55]. As shown in Supporting Information Fig. S20, a significant decrease in liposome uptake was observed at 4 °C, confirming that liposomes primarily entered cells *via* active transport. In the presence of colchicine, no significant reduction in liposome uptake was observed. However, inhibition by chlorpromazine significantly reduced the absorption of liposomes across the cell membrane, indicating that clathrin-mediated adsorptive endocytosis plays a role in liposome uptake. In contrast, when filipin was used, only the uptake of SP-Lip and SRP-Lip was significantly reduced, suggesting that modification with self-peptide promoted liposome transport *via* caveolae.

In addition, we established a Transwell model of the bEnd.3 endothelial cell barrier (Supporting Information Fig. S21)[35]. Through confocal microscopy examination of cross-sectional images of the cell layers, it was evident that at the 2 h mark,

Please cite this article as: Duan Xuehui et al., Dichotomous role of CD47−SIRPα axis: Leveraging opposing functions in phagocytic resistance and transport assistance for enhanced nanocarrier biocompatibility and tumor penetration, Acta Pharmaceutica Sinica B, https://doi.org/10.1016/j.apsb.2025.11.013

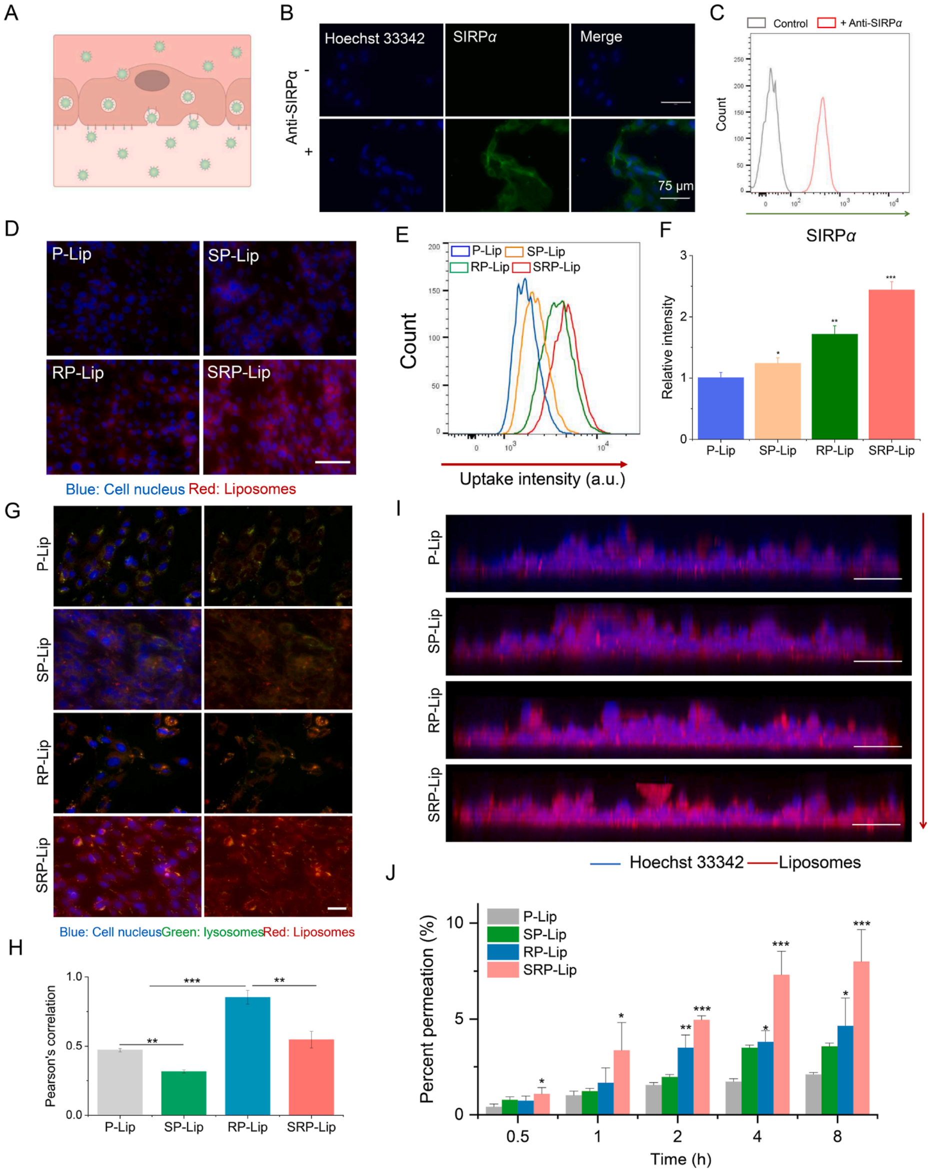

Figure 5 "Don't-eat-me" signaling mediates enhanced liposomal transcytosis across endothelial cell barriers. (A) Illustration showing the transmembrane transport of the complex formed by CD47 or CD47-derived self-peptides interacting with SIRPα. (B) Immunofluorescence and (C) flow cytometric analysis confirming the significant expression of SIRPα in endothelial bEnd.3 cells. Fluorescence imaging analysis of liposome uptake by bEnd.3 cells is shown in (D), along with a quantitative analysis *via* flow cytometry presented in (E, F). (G, H) Colocalization imaging analysis of liposomes and SIRPα. (I) Confocal section imaging demonstrating the traversal of liposomes across the bEnd.3 cell layer, scale bars = 50 μm. (J) Analysis of the ratio of liposomes traversing the bEnd.3 cell layer. Data are presented as the mean ± SD ($n = 3$), $^{*}P < 0.05$, $^{**}P < 0.01$, and $^{***}P < 0.001$.

the permeability of SRP-Lip surpassed that of both RP-Lip and SP-Lip (Fig. 5I). When delving into the quantitative assessment of permeability dynamics using the Transwell system, we found that within the initial 30 min interval, SRP-Lip displayed a statistically significant elevation in permeation rates compared to P-Lip. Meanwhile, RP-Lip and SP-Lip exhibited a minor, albeit statistically insignificant, increase in permeability compared to P-Lip. Importantly, SRP-Lip maintained a consistent and statistically notable increase in permeability over time (Fig. 5J). Collectively, these findings provide a mechanistic insight: the RGD peptide, by augmenting the affinity between liposomes and endothelial cell membranes, and the self-peptide, by stimulating liposomal transcytosis, act in concert to amplify liposomes across the endothelial cell barrier. This synergy highlights the potential of SRP-Lip as an advanced delivery vehicle capable of more effectively navigating the complex microenvironment of the vasculature, thus enhancing the efficiency of drug delivery to target sites.

3.6. *Liposome hitchhiking on macrophages to penetrate tumor spheres based on CD47-SIRPα axis*

Following the traversal of blood vessels, the heterogeneity of the tumor microenvironment becomes a pivotal determinant of liposomal delivery efficacy. Therefore, we investigated the effect of

Please cite this article as: Duan Xuehui et al., Dichotomous role of CD47−SIRPα axis: Leveraging opposing functions in phagocytic resistance and transport assistance for enhanced nanocarrier biocompatibility and tumor penetration, Acta Pharmaceutica Sinica B, https://doi.org/10.1016/j.apsb.2025.11.013

the current delivery system on the interactions between liposomes and tumor cells. The 4T1 cell line, a mouse breast cancer cell line was used to assess the uptake of liposomes after a 2 h culture period. Given that $\alpha_v\beta_3$ integrin is also highly expressed in 4T1 cells (Supporting Information Fig. S22), rendering the RGD peptide a potent facilitator of liposome-cell engagement. Consequently, RP-Lip and SRP-Lip, leveraging the RGD moiety, demonstrated significantly elevated uptake compared to their P-Lip and SP-Lip counterparts (Fig. 6A−C).

Doxorubicin hydrochloride (DOX), a common chemotherapeutic agent, is widely used in the clinical settings[56]. Traditional doxorubicin has a large volume of distribution, tending to spread extensively throughout various tissues and organs in the body, leading to toxicity in normal tissues. In contrast, doxorubicin-loaded liposomes, such as PEGylated liposomes, can remain in the circulation for a longer period and possess stealth characteristics, making them less detectable by the mononuclear phagocyte system. This allows the drug to concentrate more effectively around tumor tissues, reducing its distribution to normal tissues such as the heart, liver, and kidneys, thereby decreasing toxicity to these organs[57,58]. We used DOX as a model drug and tested its encapsulation rate and stability. The encapsulation rate of DOX in different groups was ∼90% (Supporting Information Table S5), and the particle size and drug loading did not change significantly when stored at 4 °C for 7 days (Supporting Information Fig. S23). We then evaluated 4T1 cell death in different liposome groups by performing the MTT assay (Fig. 6D, Supporting Information Fig. S24). Notably, RP-Lip/DOX and SRP-Lip/DOX exhibited comparable IC_{50} values, which were significantly lower than those of P-Lip/DOX and SP-Lip/DOX formulations (Fig. 6D). In addition, we observed a significant upregulation of $\alpha_v\beta_3$ integrin on the surface of M2 macrophages compared to M1 macrophages, thereby enhancing the selective targeting efficiency of RP-Lip and SRP-Lip in these cells (Supporting Information Figs. S25-S27) [59].

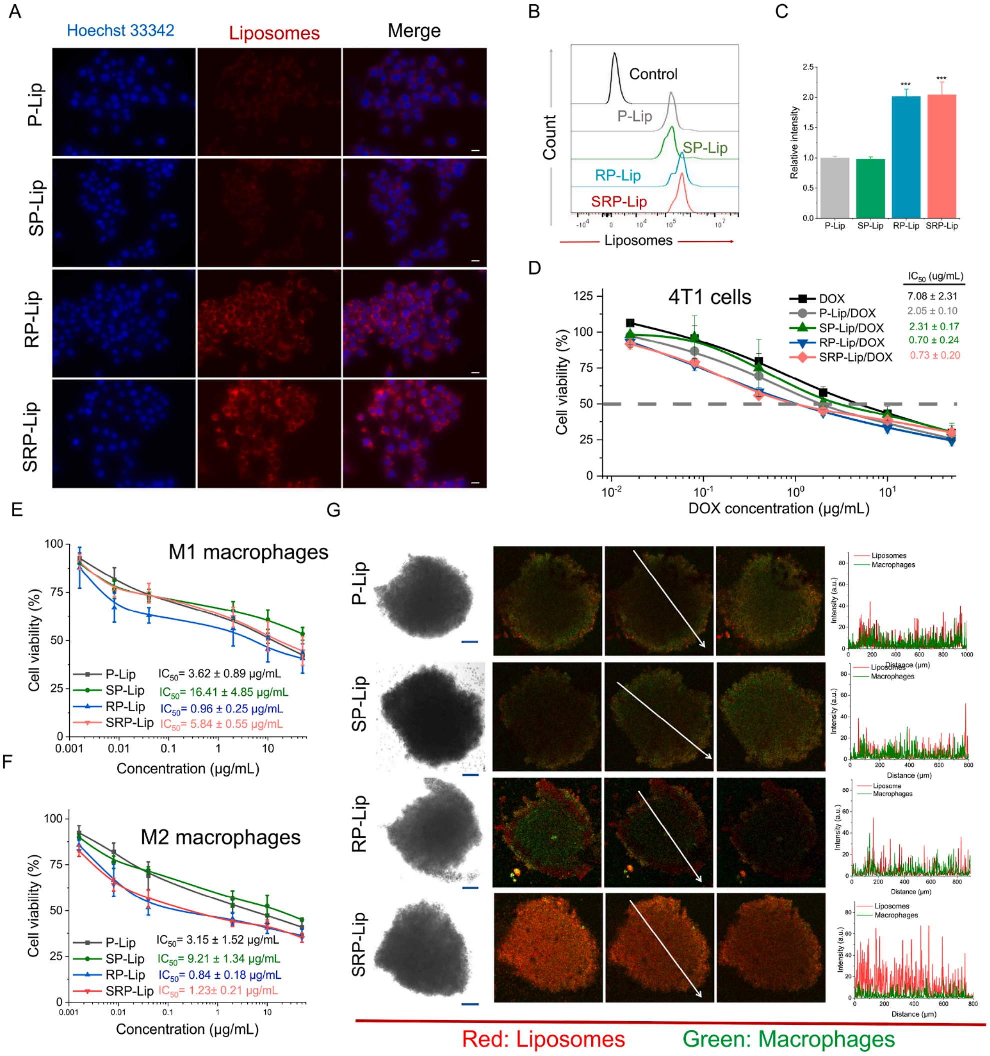

Figure 6 Self-peptide enhances liposome penetration in 4T1 cells. (A) Fluorescence imaging of liposome uptake by 4T1 cells; liposomes were pre-incubated with cells for 2 h and observed using fluorescence microscopy. (B) and (C) Flow cytometric analysis of liposome uptake by 4T1 cells. (D) Cytotoxicity of doxorubicin (DOX)/DOX-loaded liposomes toward 4T1 cells. Cytotoxicity of doxorubicin (DOX)/DOX-loaded liposomes toward (E) M1-type macrophages and (F) M2-type macrophages. (G) Penetration of liposomes into 4T1 tumor spheroids. Tumor spheroids were incubated with various liposomes for 2 h in a medium containing 10% FBS. Images were captured at intervals of 30 μm from the top to the bottom of the live spheroids. Scale bar = 100 μm. Data are shown as the mean ± SD ($n = 3$), $^*P < 0.05$, $^{**}P < 0.01$, and $^{***}P < 0.001$.

Please cite this article as: Duan Xuehui et al., Dichotomous role of CD47−SIRPα axis: Leveraging opposing functions in phagocytic resistance and transport assistance for enhanced nanocarrier biocompatibility and tumor penetration, Acta Pharmaceutica Sinica B, https://doi.org/10.1016/j.apsb.2025.11.013

Previous research has demonstrated that "don't-eat-me" signals, such as CD47, are more effective in inhibiting phagocytosis by M1 macrophages compared to M2 macrophages[36,38]. To further validate the selective targeting capabilities of SRP-Lip and RP-Lip, we evaluated their cytotoxicity against M1 and M2 macrophages. The IC_{50} values for SRP-Lip/DOX were found to be 5.84 ± 0.55 μg/mL for M1 macrophages and 1.23 ± 0.21 μg/mL for M2 macrophages. In contrast, the IC_{50} values for RP-Lip/DOX were 0.96 ± 0.25 μg/mL for M1 macrophages and 0.84 ± 0.18 μg/mL for M2 macrophages (Fig. 6E and F). These results indicate that SRP-Lip/DOX exhibits higher selectivity toward M2 macrophages, with a nearly five-fold difference in IC_{50} values between M1 and M2 macrophages. This selectivity is likely due to the combined effects of $\alpha_v\beta_3$ integrin upregulation and the reduced inhibitory signals in M2 macrophages, which facilitate the efficient internalization and subsequent cytotoxicity of SRP-Lip/DOX.

Following nanoparticle extravasation, they must traverse the intricate microenvironment of solid tumors. It is widely recognized that diffusion is the primary mechanism through which nanoparticles are distributed within tumors[18]; however, this process is impeded by a dense extracellular matrix. Furthermore, the activities of tumor-associated macrophages (TAMs), which can redistribute nanoparticles, introduce another layer of complexity into nanoparticle trafficking. Given that the RGD peptide fosters adherence to macrophage surfaces and the CD47-SIRPα "don't-eat-me" signal inhibits macrophage-mediated liposome endocytosis, we posited that SRP-Lip might proficiently infiltrate the tumor milieu *via* a macrophage-assisted transport mechanism.

To validate this hypothesis, we utilized a 4T1 cell-based model to generate tumor spheroids, both with and without the presence of fluorescently labeled RAW264.7 macrophages (as visualized in green). As illustrated in (Fig. 6G, Supporting Information Fig. S28), all liposome types accumulated around the periphery of the tumor spheroids devoid of macrophages. Intriguingly, in spheroids co-cultured with RAW264.7, SRP-Lip demonstrated a pronounced increase in accumulation at the spheroid cores, accompanied by striking colocalization of the red fluorescence of SRP-Lip with the green fluorescence of macrophages. This compelling evidence supports our contention that RAW264.7 macrophages facilitate the deep penetration of SRP-Lip into the tumor mass.

3.7. *Liposomes based on "don't-eat-me" signaling hitchhike macrophages to achieve deep penetration and delivery in tumors*

Following the establishment of subcutaneous tumors using 4T1 cells, we confirmed the expression of SIRPα in the tumor vasculature (Supporting Information Fig. S29). For *in vivo* tracking, DiR-labeled liposomes were prepared and injected. At 1 h, the SRP-Lip and RP-Lip groups demonstrated comparable tumor distributions, which were slightly higher than those of the SP-Lip and P-Lip groups, respectively. However, over time, the accumulation of SRP-Lip in the tumor increased rapidly and was significantly greater than that of RP-Lip (Fig. 7A and B).

To delve deeper into understanding and visually depict the localization of liposomes within the tumor milieu, sections of tumors were meticulously prepared. As revealed in (Fig. 7C and D, Supporting Information Figs. S30 and S31), both RP-Lip and SRP-Lip displayed heightened fluorescence intensity within the tumor areas, confirming their augmented accumulation at the tumor site. Notably, SRP-Lip demonstrated a markedly elevated level of colocalization with macrophages, implying a proficient engagement with these cells upon infiltration into the tumor parenchyma. In contrast, RP-Lip showed a prominent association with endothelial cells, suggesting that its infiltration into the tumor mass might be largely confined to the vicinity of blood vessels. SRP-Lip, on the other hand, exhibited a more homogeneous dispersion throughout the tumor and a reduced degree of colocalization with endothelial cells. This pattern indicates a superior capacity of SRP-Lip to disperse freely within the tumor tissue, thereby enhancing drug release directly into the tumor parenchyma, which is imperative for therapeutic efficacy.

To further scrutinize the depth of liposome infiltration into the tumor architecture, tumor samples were harvested 24 h post-administration of DiI-labeled liposomes. Following processing *via* the BBAB protocol, light microscopy imagery illustrated that SRP-Lip penetrated to significantly greater depths than other liposomal formulations within the tumors and achieved a more comprehensive dispersion across the tumor tissue (Fig. 7E).

Additionally, we analyzed the interaction of liposomes with M1 macrophages, M2 macrophages, T cells, and myeloid-derived suppressor cells (MDSCs) in the tumors (Fig. 7F and G, Supporting Information Fig. S32). Our findings revealed that SRP-Lip and RP-Lip displayed a significantly elevated affinity for M2 macrophages compared to P-Lip. Considering the role of M1 macrophages in fostering inflammation and anti-tumor responses[60,61], and conversely, M2 macrophages' pro-tumorigenic actions and immunosuppressive effects[62], this selective targeting may facilitate the selective clearance of M2 macrophages, thereby rebalancing the tumor immune landscape toward a more anti-tumor state. Moreover, the augmented presence of SRP-Lip-positive T cells and MDSCs implies active modulation of the tumor immune microenvironment by SRP-Lip, which could further potentiate the therapeutic effect on the tumor.

3.8. *Synergistic modification of "don't-eat-me" signaling and PEG promotes liposome delivery to tumors and therapeutic effects*

To evaluate the potential role of SRP-Lip in anti-tumor therapy, we used a 4T1 subcutaneous tumor model for *in vivo* pharmacological analysis. Mice with established tumors were administered PBS, DOX (5 mg DOX/kg), or DOX-loaded liposomes (5 mg DOX/kg) weekly for 2 weeks. On the Day 14, the mice were euthanized for further analysis (Fig. 8A).

SRP-Lip inhibited tumor progression more significantly than PBS and the other administered treatments (Fig. 8B and C). Compared with that in the PBS group, the inhibition rate reached approximately ∼20%, whereas the inhibition rate in the SP-Lip and RP-Lip groups was only approximately ∼50%. We then removed the tumors under the skin from the mice in each group and weighed them (Fig. 8D and E). During the treatment period, the weight of the mice treated with RP-Lip/DOX decreased slightly; however, when treatment was terminated, the weight returned to normal (Fig. 8F). This suggests that liposomes in each group had controlled toxicity.

Our investigation was extended to examine the impact of various treatments on the tumor immune microenvironment. Histological assessments using H&E staining, coupled with Tunel assays, revealed a conspicuous surge in apoptotic tumor cells

Please cite this article as: Duan Xuehui et al., Dichotomous role of CD47−SIRPα axis: Leveraging opposing functions in phagocytic resistance and transport assistance for enhanced nanocarrier biocompatibility and tumor penetration, Acta Pharmaceutica Sinica B, https://doi.org/10.1016/j.apsb.2025.11.013

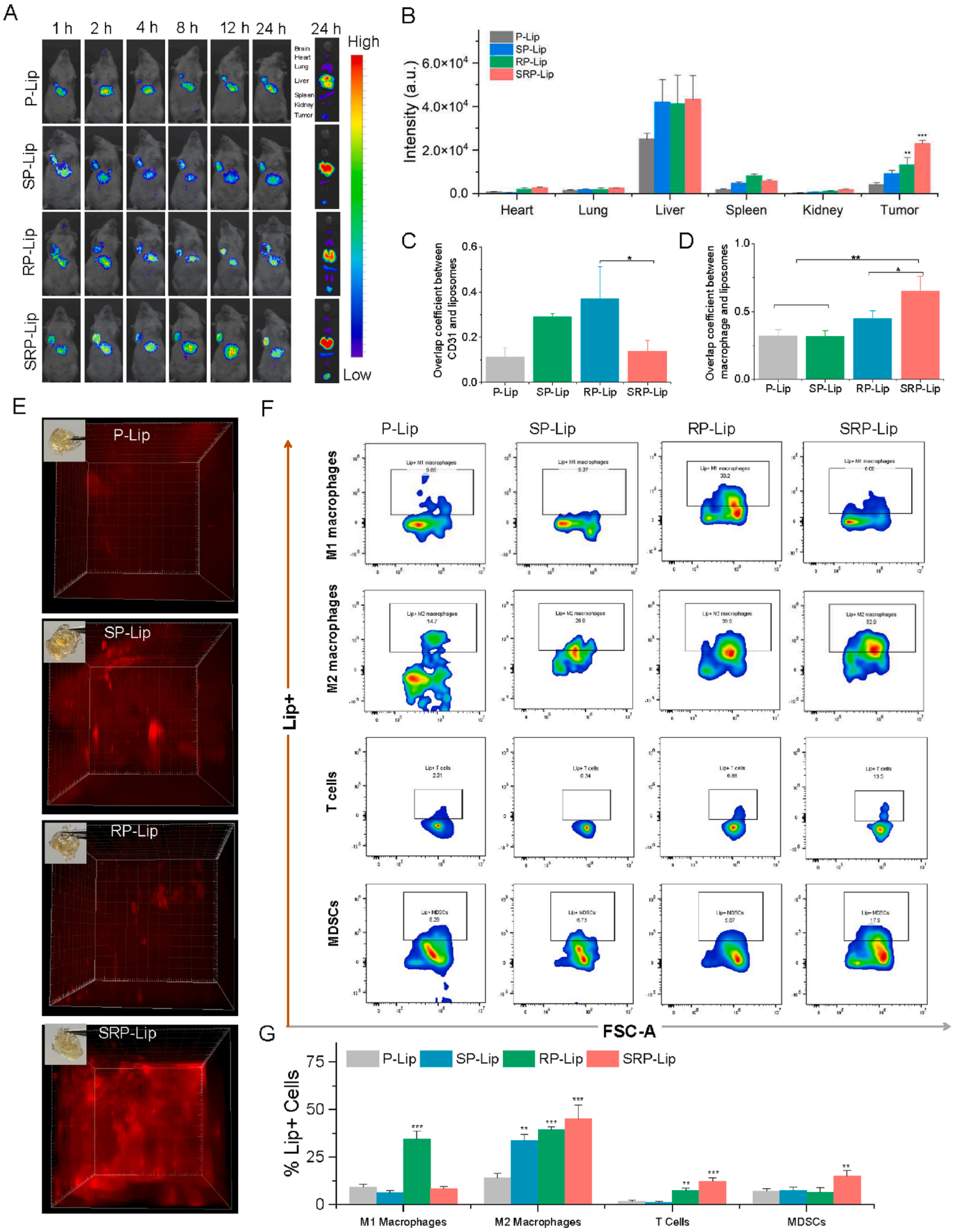

Figure 7 Self-peptides enhance liposomal targeting and penetration at tumor sites. (A) In vivo and ex vivo tracing of liposomes after intravenous injection. (B) Region of interest (ROI) quantification of major organs in mice 24 h after the intravenous injection of liposomes. (C) Overlap coefficient of liposomes with endothelial cells and associated liposomes. (D) Overlap coefficient of liposomes with macrophages. DiI-labeled liposomes were injected *via* the tail vein, followed by tumor section analysis 24 h post-injection. (E) Microscopic 3D imaging of liposome distribution in tumor tissues after tumor clarification. (F) and (G) show the colocalization of liposomes with M1 macrophages, M2 macrophages, T cells, and myeloid-derived suppressor cells (MDSCs) in the tumor 4 h post-DiI-labeled liposome injection (50 mg/kg) *via* the tail vein. Data are presented as the mean ± SD ($n = 3$), $^{*}P < 0.05$, $^{**}P < 0.01$, and $^{***}P < 0.001$.

within the SRP-Lip/DOX cohort, pointing to a heightened therapeutic efficacy in inducing tumor cell death (Fig. 9A).

Delving deeper into the tumor's immune landscape (Fig. 9B, Supporting Information Fig. S33A), macrophages are predominant immune constituents in tumors, and displayed a remarkable shift in polarization (Fig. 9C, Fig. S33B and S33C). M1 macrophages, known for their tumor-destructive capabilities, showed a statistically significant rise in the SRP-Lip/DOX group, paralleled by a substantial decline in M2 macrophages, which foster tumor progression and metastasis (Fig. 9C)[61-63]. This skewed balance toward the M1 phenotype, reflected in an elevated M1/M2 ratio (1.77 for SRP-Lip/DOX and 1.53 for SP-Lip). TAM is also important for regulating the number of other immune cells in the tumor. For example, they inhibit T-cell activity and activate

Please cite this article as: Duan Xuehui et al., Dichotomous role of CD47−SIRPα axis: Leveraging opposing functions in phagocytic resistance and transport assistance for enhanced nanocarrier biocompatibility and tumor penetration, Acta Pharmaceutica Sinica B, https://doi.org/10.1016/j.apsb.2025.11.013

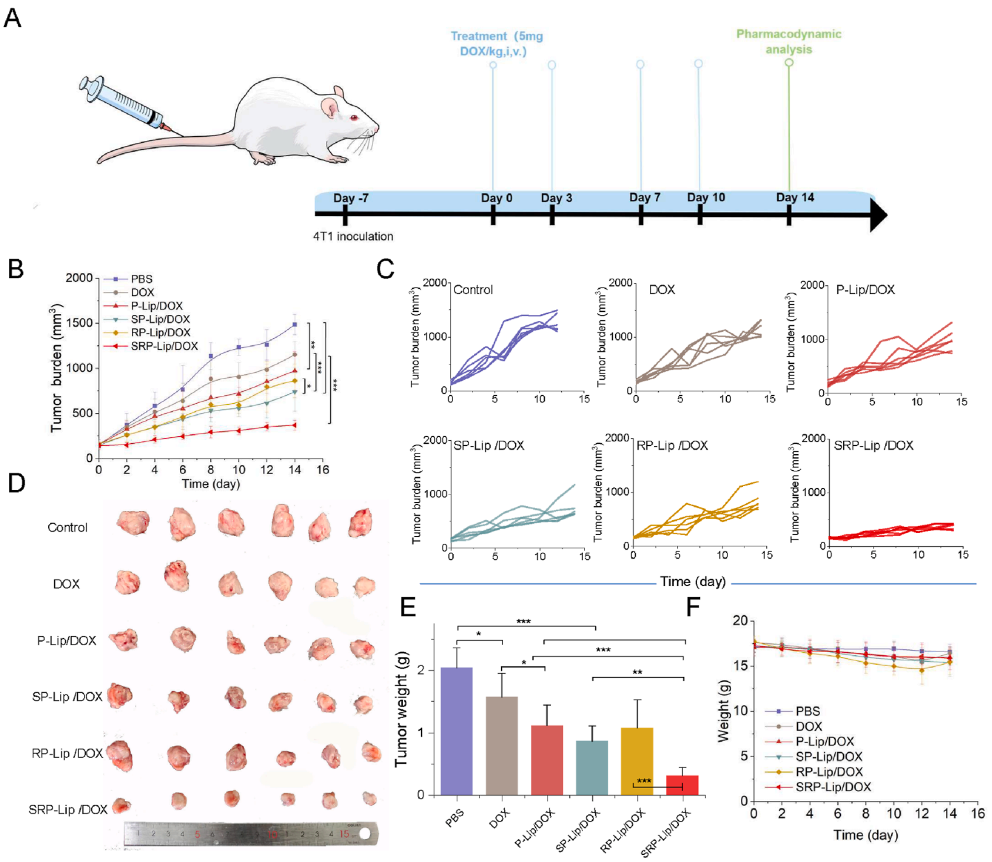

Figure 8 Anti-tumor efficacy of SRP-Lip/DOX (doxorubicin) against subcutaneous 4T1 tumors. (A) Schematic representation illustrating the treatment procedure administered to BALB/c mice with 4T1 subcutaneous tumors, receiving either PBS/DOX/DOX-loaded liposomes at days 0, 3, 7, and 10. Histological and biochemical analyses were performed on day 14. (B) Growth curves of 4T1 tumors after the intravenous injection of PBS, DOX, and DOX-loaded liposomes. (C) Tumor volume growth curves for each mouse in the different treatment groups. (D) Images of tumors extracted from mice. (E) Average tumor weight for each group at the end of the experiment. (F) Variation in the body weights of tumor-bearing mice during treatment. Data are presented as the mean ± SD. Data are presented as the mean ± SD ($n = 6$), $^{*}P < 0.05$, $^{**}P < 0.01$, and $^{***}P < 0.001$.

MDSCs[23,64,65]. T cells play a crucial role in tumor cytotoxicity, and their prevalence is a critical determinant of tumor therapy. As shown in (Fig. S33B and S33D), the infiltration numbers of T cells in RP-Lip and SRP-Lip were all significantly increased. In the SRP-Lip/DOX cohort, both the proportions of CD4+ and CD8+ T cells were notably higher compared to the PBS group (Fig. 9D). Regulatory T cells (Tregs), which dampen the activity of immune effector cells like CD8+ T cells and natural killer cells, were found to be significantly less numerous in the SRP-Lip/DOX group compared to other treatments (Fig. 9E). This attenuation of Tregs signifies successful reprogramming of the tumor microenvironment following SRP-Lip/DOX infiltration and drug delivery, promoting an immune milieu that is more conducive to tumor eradication. Lastly, MDSCs exhibit robust immunosuppressive properties. Notably, both Granulocytic (G)-MDSC and Monocytic (M)-MDSC subpopulations were significantly reduced in the SRP-Lip/DOX group (Fig. 9F).

In addition to therapeutic efficacy, we meticulously assessed the safety profile of the delivery vehicles. Histological assessments *via* H&E and Tunel staining indicated a favorable safety profile for DOX-encapsulated liposomes (Supporting Information Figs. S34 and S35). We carried out a serum biochemical analysis on mice after administration (Supporting Information Fig. S36), focusing on key markers indicating liver function, namely alanine aminotransferase (ALT) and aspartate aminotransferase (AST), and renal function evaluated by creatinine (Cr). Our results show that mice treated with Lip/DOX did not present statistically significant changes in these crucial biochemical parameters compared to the blank control group, indicating that within the time limit of our study, this formulation did not cause noticeable systemic toxic effects. Repeated localized injections can lead to overactivation of the immune system owing to persistent stimulation, resulting in inflammatory responses. At the injection site, immune cells, such as macrophages and neutrophils, accumulate and secrete pro-inflammatory cytokines, which can cause local tissue damage. Repeated administration of doxorubicin (DOX) induces erythema, edema, severe pain, and potential skin ulceration at the injection site[66]. As modifying carriers with the CD47-SIRPα axis reduced the activation of the immune system, our investigation demonstrated that mice administered SRP-Lip/DOX and SP-Lip/DOX exhibited improved tail conditions compared to those receiving unmodified formulations. Furthermore, tunel assays revealed a significant increase in apoptotic events in the tail cells of mice treated with

Please cite this article as: Duan Xuehui et al., Dichotomous role of CD47−SIRPα axis: Leveraging opposing functions in phagocytic resistance and transport assistance for enhanced nanocarrier biocompatibility and tumor penetration, Acta Pharmaceutica Sinica B, https://doi.org/10.1016/j.apsb.2025.11.013

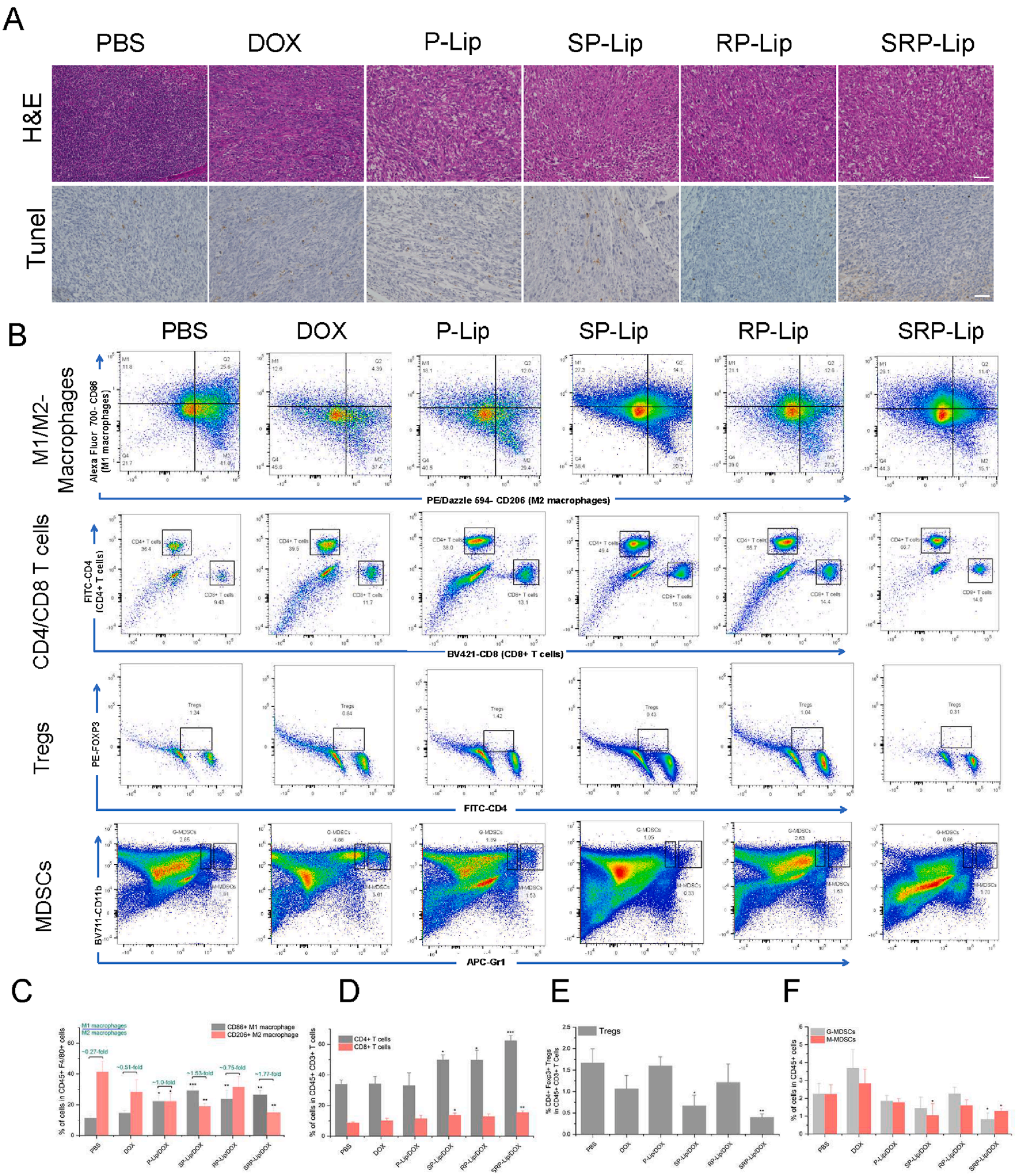

Figure 9 Differential regulation of the tumor microenvironment after treatment with various drugs. (A) H&E and Tunel staining of tumor sections, scale bars = 100 μm. (B) Flow cytometry utilized to identify different tumor cell fractions. (C) Flow cytometry analysis of CD45+ F4/80+ CD86+ M1 and CD45+ F4/80+ CD206+ M2 macrophages. (D) Flow cytometry analysis of CD45+ CD3+ CD4+ T cells and CD45+ CD3+ CD8+ T cells. (E) Flow cytometry analysis of tumor-infiltrating CD4+ Foxp3+ Treg cells. (F) Flow cytometry analysis of tumor-infiltrating Gr1 high CD11b + granulocytes (G-MDSCs) and Gr1int CD11b + monocytes (M-MDSCs). Data are shown as the mean ± SD ($n = 3$), *$P < 0.05$, **$P < 0.01$, and ***$P < 0.001$ versus the PBS group.

RP-Lip, indicating local toxicity (Supporting Information Fig. S37). Conversely, incorporation of self-peptides into SRP-Lip mitigated these adverse effects, supporting the hypothesis that this modification enhances immunological compatibility and reduces toxicity *in vivo*, thereby contributing to a safer therapeutic approach.

4. Conclusions

In conclusion, it is evident that CD47 has emerged as a key stone in the progression of biocompatible, high-performance biomimetic systems for drug delivery, primarily owing to its critical interaction with macrophage-expressed SIRPα that instigates a vital “don’t-eat-me” signal. Conventionally, PEGylation techniques have been favored for prolonging circulation times by impeding macrophage uptake and reducing hepatic accumulation of therapeutic formulations. Nonetheless, when considering delivery systems that usethe CD47−SIRPα axis, these conventional methods prove less effective owing to fundamentally different operational mechanisms; PEG’s protective effect stems from physical barriers formed by hydrophilic chains, whereas the “don’t-eat-me” signaling reaches its apex during macrophage endocytosis of surface-anchored liposomes. Our investigation into the interplay between self-peptide liposomes and macrophages has highlighted the unique characteristics of a “don’t-eat-me”-centered delivery system and its intricate macrophage interactions.

Although surface hydrophilic polymer coatings, epitomized by PEGylation, excel in minimizing plasma protein adsorption and promoting safer, more efficient *in vivo* delivery, recurrent dosing encounters the challenge of ABC, resulting in swift macrophage-mediated elimination of PEGylated materials following detection by IgM. By using the CD47−SIRPα axis’s established ability to inhibit macrophage phagocytosis through its “don’t-eat-me” signaling, we have demonstrated its effectiveness in reducing plasma protein-mediated macrophage recognition, accelerating the clearance of PEGylated liposomes, and inhibiting antibody deposition and complement activation on carrier surfaces. This strategy further employs macrophages for enhanced tumor infiltration and microenvironment modulation, leading to a substantial amplification of therapeutic outcomes. These findings elucidate the critical importance of “don’t-eat-me” signaling in determining carrier biocompatibility and delivery efficiency, enriching the repertoire for designing secure and efficient delivery vehicles using innovative materials.

Additionally, while the CD47−SIRPα axis has long been lauded recognized for suppressing macrophage-mediated cytostasis, its potential in modulating endothelial cell dynamics has remained relatively unexplored. Our current study has revealed a critical function of this axis in mediating the traversal of delivery vehicles across the endothelial barrier. Notably, while solitary CD47−SIRPα modification yields minimal enhancements in *trans*-endothelial transport, combination with the RGD peptide significantly boosts liposome passage. This cooperative action not only promotes transmembrane shuttling of liposomes but also alleviates post-endocytic lysosomal sequestration, thereby expanding our understanding of the multifaceted role of the CD47−SIRPα axis in orchestrating *in vivo* carrier delivery and highlighting its substantial potential in advancing biomedical applications.

Acknowledgments

This work was supported by the Shandong Natural Science Foundation (ZR2021MH118, China), Shandong Province Medical and Health Science and Technology Project (202413020649, China), Special funds for Taishan Scholars Project (tsqnz20221156, tsqn202306383, China), and academic promotion program of Shandong First Medical University (2019LJ003, China).

Author contributions

Xuehui Duan: Data curation, Writing − original draft, Methodology. Yixuan Tang: Resources, Conceptualization, Supervision, Funding acquisition, Visualization, Methodology, Data curation. Zhongjie Tang: Methodology, Data curation. Yan Du: Methodology, Data curation. Xinlei Chu: Data curation, Methodology. Xin-Long Liu: Data curation, Methodology. Zhanyan Liu: Data curation, Methodology. Kun Zhao: Data curation, Visualization, Resources. Wei Xu: Data curation, Funding acquisition, Visualization. Chong Li: Visualization, Methodology, Conceptualization, Supervision, Writing − original draft, Resources, Funding acquisition.

Conflicts of interest

The authors have no conflicts of interest to declare.

Appendix A. Supporting information

Supporting information to this article can be found online at https://doi.org/10.1016/j.apsb.2025.11.013.

References

1. Wang FH, Huang Q, Su H, Sun MJ, Wang ZY, Chen ZQ, et al. Self-assembling paclitaxel-mediated stimulation of tumor-associated macrophages for postoperative treatment of glioblastoma. *Proc Natl Acad Sci U S A* 2023;**120**:e2090346176.
2. Luo M, Wang H, Wang ZH, Cai HC, Lu ZG, Li Y, et al. A STING-activating nanovaccine for cancer immunotherapy. *Nat Nanotechnol* 2017;**12**:648−54.
3. Zhao DY, Tao WH, Li SH, Chen Y, Sun YH, He ZG, et al. Apoptotic body-mediated intercellular delivery for enhanced drug penetration and whole tumor destruction. *Sci Adv* 2021;**7**:eabg0880.
4. Tang HL, Xu XJ, Chen YX, Xin HH, Wan T, Li BW, et al. Reprogramming the tumor microenvironment through second-near-infrared-window photothermal genome editing of PD-L1 mediated by supramolecular gold nanorods for enhanced cancer immunotherapy. *Adv Mater* 2021;**33**:e2006003.
5. Zhou Q, Shao SQ, Wang JQ, Xu CH, Xiang JJ, Piao Y, et al. Enzyme-activatable polymer-drug conjugate augments tumour penetration and treatment efficacy. *Nat Nanotechnol* 2019;**14**:799−809.
6. Ouyang B, Poon W, Zhang YN, Lin ZP, Kingston BR, Tavares AJ, et al. The dose threshold for nanoparticle tumour delivery. *Nat Mater* 2020;**19**:1362−71.
7. Li C, Wang JC, Wang YG, Gao HL, Wei G, Huang YZ, et al. Recent progress in drug delivery. *Acta Pharm Sin B* 2019;**9**:1145−62.
8. Yona S, Gordon S. From the reticuloendothelial to mononuclear phagocyte system - the unaccounted years. *Front Immunol* 2015;**6**:328.
9. Zou ZJ, Li H, Yu K, Ma K, Wang QG, Tang JN, et al. The potential role of synovial cells in the progression and treatment of osteoarthritis. *Explorations* 2023;**3**:20220132.
10. Zeng ZP, Tan RC, Chen S, Chen HL, Liu ZJ, Liu LX, et al. Di-PEGylated insulin: a long-acting insulin conjugate with superior safety in reducing hypoglycemic events. *Acta Pharm Sin B* 2024;**14**:2761−72.
11. Ishida T, Kiwada H. Accelerated blood clearance (ABC) phenomenon upon repeated injection of PEGylated liposomes. *Int J Pharm* 2008;**354**:56−62.
12. Mima Y, Hashimoto Y, Shimizu T, Kiwada H, Ishida T. Anti-PEG igm is a major contributor to the accelerated blood clearance of polyethylene glycol-conjugated protein. *Mol Pharm* 2015;**12**:2429−35.
13. Inglut CT, Sorrin AJ, Kuruppu T, Vig S, Cicalo J, Ahmad H, et al. Immunological and toxicological considerations for the design of liposomes. *Nanomaterials* 2020;**10**:190.
14. Wang H, Jiang ZX, Guo ZW, Luo G, Ding TH, Zhan CY. mIgM-mediated splenic marginal zone B cells targeting of folic acid for immunological evasion. *Acta Pharm Sin B* 2024;**14**:808−20.

Please cite this article as: Duan Xuehui et al., Dichotomous role of CD47−SIRPα axis: Leveraging opposing functions in phagocytic resistance and transport assistance for enhanced nanocarrier biocompatibility and tumor penetration, Acta Pharmaceutica Sinica B, https://doi.org/10.1016/j.apsb.2025.11.013

15. Zhang YR, Lin R, Li HJ, He WL, Du JZ, Wang J. Strategies to improve tumor penetration of nanomedicines through nanoparticle design. *Wiley Interdiscip Rev Nanomed Nanobiotechnol* 2019;**11**: e1519.
16. Chen SQ, Zhong Y, Fan WF, Xiang JJ, Wang GW, Zhou Q, et al. Enhanced tumour penetration and prolonged circulation in blood of polyzwitterion−drug conjugates with cell-membrane affinity. *Nat Biomed Eng* 2021;**5**:1019−37.
17. Yan Y, Chen BL, Yin QQ, Wang ZH, Yang Y, Wan FJ, et al. Dissecting extracellular and intracellular distribution of nanoparticles and their contribution to therapeutic response by monochromatic ratiometric imaging. *Nat Commun* 2022;**13**:2004.
18. Shi Y, van der Meel R, Chen XY, Lammers T. The epr effect and beyond: strategies to improve tumor targeting and cancer nanomedicine treatment efficacy. *Theranostics* 2020;**10**:7921−4.
19. Sindhwani S, Syed AM, Ngai J, Kingston BR, Maiorino L, Rothschild J, et al. The entry of nanoparticles into solid tumours. *Nat Mater* 2020;**19**:566−75.
20. Javid H, Oryani MA, Rezagholinejad N, Esparham A, Tajaldini M, Karimi-Shahri M. Rgd peptide in cancer targeting: benefits, challenges, solutions, and possible integrin-RGD interactions. *Cancer Med* 2024;**13**:e6800.
21. Zhang QY, Lu LB, Zhang L, Shi KR, Cun XL, Yang YT, et al. Dual-functionalized liposomal delivery system for solid tumors based on RGD and a pH-responsive antimicrobial peptide. *Sci Rep* 2016;**6**: 19800.
22. Shen XD, Pan DY, Gong QY, Gu ZW, Luo K. Enhancing drug penetration in solid tumors *via* nanomedicine: evaluation models, strategies and perspectives. *Bioact Mater* 2023;**32**:445−72.
23. Munir MU. Nanomedicine penetration to tumor: challenges, and advanced strategies to tackle this issue. *Cancers (Basel)* 2022;**14**: 2904.
24. Ye ZH, Yu WB, Huang MY, Chen J, Lu JJ. Building on the backbone of CD47-based therapy in cancer: combination strategies, mechanisms, and future perspectives. *Acta Pharm Sin B* 2023;**13**: 1467−87.
25. Rodriguez PL, Harada T, Christian DA, Pantano DA, Tsai RK, Discher DE. Minimal "self" peptides that inhibit phagocytic clearance and enhance delivery of nanoparticles. *Science* 2013;**339**:971−5.
26. Oldenborg PA, Zheleznyak A, Fang YF, Lagenaur CF, Gresham HD, Lindberg FP. Role of CD47 as a marker of self on red blood cells. *Science* 2000;**288**:2051−4.
27. Ren BY, Xia H, Liao YJ, Zhou H, Wang ZN, Shi YY, et al. Endothelial sirpalpha signaling controls VE-cadherin endocytosis for thymic homing of progenitor cells. *eLife* 2022;**11**:e69219.
28. de Vries HE, Hendriks JJ, Honing H, De Lavalette CR, van der Pol SM, Hooijberg E, et al. Signal-regulatory protein alpha-CD47 interactions are required for the transmigration of monocytes across cerebral endothelium. *J Immunol* 2002;**168**:5832−9.
29. Kusakari S, Ohnishi H, Jin FJ, Kaneko Y, Murata T, Murata Y, et al. Trans-endocytosis of CD47 and shps-1 and its role in regulation of the cd47-shps-1 system. *J Cell Sci* 2008;**121**:1213−23.
30. Lai JL, Pan Q, Chen GH, Liu Y, Chen C, Pan YW, et al. Triple hybrid cellular nanovesicles promote cardiac repair after ischemic reperfusion. *ACS Nano* 2024;**18**:4443−55.
31. Lin ZP, Nguyen LNM, Ouyang B, Macmillan P, Ngai J, Kingston BR, et al. Macrophages actively transport nanoparticles in tumors after extravasation. *ACS Nano* 2022;**16**:6080−92.
32. Tang YX, Wang XY, Li J, Nie Y, Liao GJ, Yu Y, et al. Overcoming the reticuloendothelial system barrier to drug delivery with a "don't-eat-us" strategy. *ACS Nano* 2019;**13**:13015−26.
33. Kucuksayan E, Bozkurt F, Yilmaz MT, Sircan-Kucuksayan A, Hanikoglu A, Ozben T. A new combination strategy to enhance apoptosis in cancer cells by using nanoparticles as biocompatible drug delivery carriers. *Sci Rep* 2021;**11**:13027.
34. Guan J, Shen Q, Zhang Z, Jiang ZX, Yang Y, Lou MQ, et al. Enhanced immunocompatibility of ligand-targeted liposomes by attenuating natural igm absorption. *Nat Commun* 2018;**9**:2982.
35. Li GL, Simon MJ, Cancel LM, Shi ZD, Ji XY, Tarbell JM, et al. Permeability of endothelial and astrocyte cocultures: *in vitro* blood−brain barrier models for drug delivery studies. *Ann Biomed Eng* 2010;**38**:2499−511.
36. Qie YQ, Yuan HF, von Roemeling CA, Chen YX, Liu XJ, Shih KD, et al. Surface modification of nanoparticles enables selective evasion of phagocytic clearance by distinct macrophage phenotypes. *Sci Rep* 2016;**6**:26269.
37. Dodt HU, Leischner U, Schierloh A, Jahrling N, Mauch CP, Deininger K, et al. Ultramicroscopy: three-dimensional visualization of neuronal networks in the whole mouse brain. *Nat Methods* 2007;**4**: 331−6.
38. Tang YX, Tang ZJ, Li PR, Tang KC, Ma ZY, Wang YT, et al. Precise delivery of nanomedicines to M2 macrophages by combining "eat me/don't eat me" signals and its anticancer application. *ACS Nano* 2021;**15**:18100−12.
39. Miller CR, Bondurant B, Mclean SD, Mcgovern KA, O'Brien DF. Liposome-cell interactions *in vitro*: effect of liposome surface charge on the binding and endocytosis of conventional and sterically stabilized liposomes. *Biochemistry* 1998;**37**:12875−83.
40. Lesniak A, Salvati A, Santos-Martinez MJ, Radomski MW, Dawson KA, Aberg C. Nanoparticle adhesion to the cell membrane and its effect on nanoparticle uptake efficiency. *J Am Chem Soc* 2013; **135**:1438−44.
41. Lorenz U. Shp-1 and shp-2 in T cells: two phosphatases functioning at many levels. *Immunol Rev* 2009;**228**:342−59.
42. Tsai RK, Discher DE. Inhibition of "self" engulfment through deactivation of myosin-II at the phagocytic synapse between human cells. *J Cell Biol* 2008;**180**:989−1003.
43. Dunkelberger JR, Song WC. Complement and its role in innate and adaptive immune responses. *Cell Res* 2010;**20**:34−50.
44. Hashimoto Y, Shimizu T, Abu Lila AS, Ishida T, Kiwada H. Relationship between the concentration of anti-polyethylene glycol (PEG) immunoglobulin m (IgM) and the intensity of the accelerated blood clearance (ABC) phenomenon against PEGylated liposomes in mice. *Biol Pharm Bull* 2015;**38**:417−24.
45. Wang LR, Su YQ, Wang XL, Liang KF, Liu MY, Tang WY, et al. Effects of complement inhibition on the ABC phenomenon in rats. *Asian J Pharm Sci* 2017;**12**:250−8.
46. Mastellos DC, Hajishengallis G, Lambris JD. A guide to complement biology, pathology and therapeutic opportunity. *Nat Rev Immunol* 2024;**24**:118−41.
47. Reis ES, Mastellos DC, Hajishengallis G, Lambris JD. New insights into the immune functions of complement. *Nat Rev Immunol* 2019;**19**: 503−16.
48. Dobo J, Kocsis A, Farkas B, Demeter F, Cervenak L, Gal P. The lectin pathway of the complement system-activation, regulation, disease connections and interplay with other (proteolytic) systems. *Int J Mol Sci* 2024;**25**:1566.
49. Kojouharova M, Reid K, Gadjeva M. New insights into the molecular mechanisms of classical complement activation. *Mol Immunol* 2010; **47**:2154−60.
50. Lubbers R, van Essen MF, van Kooten C, Trouw LA. Production of complement components by cells of the immune system. *Clin Exp Immunol* 2017;**188**:183−94.
51. Zhou Q, Li JJ, Xiang JJ, Shao SQ, Zhou ZX, Tang JB, et al. Transcytosis-enabled active extravasation of tumor nanomedicine. *Adv Drug Deliv Rev* 2022;**189**:114480.
52. Clark AJ, Davis ME. Increased brain uptake of targeted nanoparticles by adding an acid-cleavable linkage between transferrin and the nanoparticle core. *Proc Natl Acad Sci U S A* 2015;**112**: 12486−91.

Please cite this article as: Duan Xuehui et al., Dichotomous role of CD47−SIRPα axis: Leveraging opposing functions in phagocytic resistance and transport assistance for enhanced nanocarrier biocompatibility and tumor penetration, Acta Pharmaceutica Sinica B, https://doi.org/10.1016/j.apsb.2025.11.013

53. Chen F, Zhu LY, Zhang YL, Kumar D, Cao GL, Hu XL, et al. Clathrin-mediated endocytosis is a candidate entry sorting mechanism for Bombyx mori cypovirus. *Sci Rep* 2018;**8**:7268.
54. Song SL, Wang Y, Wang HM, Tian X, Zhang X, Zhang Q, et al. Fucoidan-induced reduction of lipid accumulation in foam cells through overexpression of lysosome genes. *Int J Biol Macromol* 2024;**263**:130451.
55. Schnitzer JE, Oh P, Pinney E, Allard J. Filipin-sensitive caveolae-mediated transport in endothelium: reduced transcytosis, scavenger endocytosis, and capillary permeability of select macromolecules. *J Cell Biol* 1994;**127**:1217−32.
56. Tacar O, Sriamornsak P, Dass CR. Doxorubicin: an update on anticancer molecular action, toxicity and novel drug delivery systems. *J Pharm Pharmacol* 2013;**65**:157−70.
57. Xu GQ, Yang DH, He CN, Zhong LL, Zhu JF, Shu Q, et al. Population pharmacokinetics and toxicity correlation analysis of free and liposome-encapsulated doxorubicin in Chinese patients with advanced breast cancer. *Cancer Chemother Pharmacol* 2023;**92**:181−92.
58. Zhang WJ, Deng XY, Wang LY, Wang J, Guo XT, Huang LG, et al. Poly(ferulic acid) nanocarrier enhances chemotherapy sensitivity of acute myeloid leukemia by selectively targeting inflammatory macrophages. *Chin Chem Lett* 2024;**35**:109422.
59. Liu HH, Wu QH, Liu SB, Liu LN, He Z, Liu Y, et al. The role of integrin alphavbeta3 in biphasic calcium phosphate ceramics mediated m2 macrophage polarization and the resultant osteoinduction. *Biomaterials* 2024;**304**:122406.
60. Li X, Wichai N, Wang JB, Liu XP, Yan HM, Wang Y, et al. Regulation of innate and adaptive immunity using herbal medicine: benefits for the COVID-19 vaccination. *Acupunct Herbal Med* 2022;**2**:196−206.
61. Meng QF, Tai WB, Tian MY, Zhuang XY, Pan YW, Lai JL, et al. Inhalation delivery of dexamethasone with isend nanoparticles attenuates the COVID-19 cytokine storm in mice and nonhuman primates. *Sci Adv* 2023;**9**:eadg3277.
62. Boutilier AJ, Elsawa SF. Macrophage polarization states in the tumor microenvironment. *Int J Mol Sci* 2021;**22**:6995.
63. Xu XY, Li RJ, Dong RQ, Yang YF, Wang HL, Cheng JL, et al. *In vitro* characterization and cellular uptake profiles of TAMs-targeted lipid calcium carbonate nanoparticles for cancer immunotherapy. *Acta Mater Med* 2022;**1**:400−10.
64. Christofides A, Strauss L, Yeo A, Cao C, Charest A, Boussiotis VA. The complex role of tumor-infiltrating macrophages. *Nat Immunol* 2022;**23**:1148−56.
65. Li YR, Brown J, Yu YQ, Lee D, Zhou KY, Dunn ZS, et al. Targeting immunosuppressive tumor-associated macrophages using innate T cells for enhanced antitumor reactivity. *Cancers (Basel)* 2022;**14**:2749.
66. Sato Y, Kondo M, Inagaki A, Komatsu H, Okada C, Naruse K, et al. Highly frequent and enhanced injection site reaction induced by peripheral venous injection of fosaprepitant in anthracycline-treated patients. *J Cancer* 2014;**5**:390−7.

Please cite this article as: Duan Xuehui et al., Dichotomous role of CD47−SIRPα axis: Leveraging opposing functions in phagocytic resistance and transport assistance for enhanced nanocarrier biocompatibility and tumor penetration, Acta Pharmaceutica Sinica B, https://doi.org/10.1016/j.apsb.2025.11.013